Back Analyses of Two Deep Excavations in Hong Kong Using the Mohr-Coulomb Model with Linear Elasticity and the Hardening Soil Model

Charles C L Chan, *Geotechnical Engineer, Geotechnical Engineering Office, Civil Engineering and Development Department, Hong Kong SAR Government, Hong Kong, email: clchan@cedd.gov.hk*
Derek S M Chiu, *Geotechnical Engineer, Geotechnical Engineering Office, Civil Engineering and Development Department, Hong Kong SAR Government, Hong Kong, email: derekchiu@cedd.gov.hk*
Frankie L C Lo, *Senior Geotechnical Engineer, Geotechnical Engineering Office, Civil Engineering and Development Department, Hong Kong SAR Government, Hong Kong, email: frankielclo@cedd.gov.hk*
Julian S H Kwan, *Assistant Director (Technical), Civil Engineering and Development Department, Hong Kong SAR Government, Hong Kong, email: juliankwan@cedd.gov.hk*
S W Lee, *Director, Golder Associated (HK) Ltd, Hong Kong; email: swlee@gloder.com.hk*
Alex C O Leung, *Geotechnical Engineer, Golder Associated (HK) Ltd, Hong Kong; email: aleung@golder.com.hk*

ABSTRACT: *The design of deep excavations in densely developed urban settings calls for critical assessments of the effects on sensitive receivers in the vicinity of the site. The linearly elastic, perfectly plastic Mohr-Coulomb (LEPP MC) model is one of the most commonly used soil constitutive models for numerical analysis in the routine design of deep excavation. However, it had been reported that the model may provide unrealistic predictions of excavation-induced ground movements and interactions with adjacent structures in some situations. A better understanding of the model applicability in various ground conditions would be needed. This paper presents: 1) two case histories of deep excavation for comparing the results from the LEPP MC model and the Hardening Soil (HS) model (a more advanced soil constitutive model), and 2) the sensitivity of the HS model by varying the input of stiffness parameters.*

KEYWORDS: Soil model, Back analysis, Finite element, Deep excavation.

SITE LOCATION: Geographic Database

INTRODUCTION

Hong Kong is a highly developed city. Many deep excavations are often carried out close to built-up areas. Deep excavations inevitably induce ground movements that could affect facilities nearby. The design of excavations in such an urban setting is often controlled by the estimated tolerable movement limits of nearby facilities. It is therefore important to predict realistic ground movements in the design stage for assessing the associated impact on the surroundings.

The most common approach used for modeling ground movements associated with deep excavations in Hong Kong is using a finite element analysis with perfectly plastic Mohr-Coulomb model coupled with linear elasticity (referred to as the "MC model" in this paper for brevity). However, it has been widely reported that such a linearly elastic, perfectly plastic (LEPP) model has limitations in modeling the stress path and loading/unloading stiffness experienced in the soil and may predict unrealistic movements induced by excavations (Potts & Zdravkovic, 2001; Atkinson, 2000; Clayton, 2011; Bolton et al, 2010; Dong et al, 2016). The use of a soil constitutive model that can better represent the nonlinear soil stiffness under different strain levels and stress paths is worth exploring with to the goal of obtaining a more accurate ground movement prediction for practical designs.

Before adopting the soil constitutive model for the design of a geotechnical structure, its applicability to the type of structures and the ground conditions concerned should be evaluated. This paper compares the applicability of the MC

Submitted: 7 April 2021; Published: 10 December 2021
Reference: Chan C., Chiu D., Lo F., Kwan J., Lee S., and Leung A. (2021). Back Analyses of Two Deep Excavations in Hong Kong Using the Mohr-Coulomb Model with Linear Elasticity and the Hardening Soil Model. International Journal of Geoengineering Case Histories, Volume 7, Issue 1, pp. 137-163, doi: 10.4417/IJGCH-07-01-07

model with another common soil constitutive model, the Hardening Soil (HS) model (Schanz et al., 1999; PLAXIS, 2019), that can model nonlinear soil stiffness when the ground movements associated with excavation works are estimated in Hong Kong. This paper provides a literature review of case histories investigating the use of the HS model, followed by presenting the back analyses of two local case histories in Hong Kong using the HS model and the MC model. Based on the back-analyzed models, the sensitivity of the input parameters of the HS model is investigated.

LITERATURE REVIEW

The Linearly Elastic, Perfectly Plastic Mohr-Coulomb Model

The MC model commonly used for the design of excavations in Hong Kong adopts an isotropic, linear elasticity relationship based on Hooke's Law (Figure 1). At the yield or failure point, the yield function (f) and plastic potential (g) are described in Equations [1] and [2] respectively. The model is a basic constitutive model traditionally used to predict the movement and stability of geotechnical problems. It is simple and only involves five basic input parameters, referring to Table 1.

$$f = \frac{1}{2}(\sigma_1' - \sigma_3') + \frac{1}{2}(\sigma_1' + \sigma_3')\sin\phi' - c'\cos\phi' = 0 \quad (1)$$

$$g = \frac{1}{2}(\sigma_1' - \sigma_3') + \frac{1}{2}(\sigma_1' + \sigma_3')\sin\psi' + constant \quad (2)$$

The Mohr-Coulomb failure criterion (or the Tresca criterion when $\phi' = 0$ and $c' = c_u$) is described by Equation [3].

$$(\sigma_1 - \sigma_3)_f = \frac{2c'\cos\phi' + 2\sigma'_3\sin\phi'}{1 - \sin\phi'} \quad (3)$$

It is known that the linearly elastic behavior prior to failure does not represent the true soil behavior and cannot consistently predict realistic ground deformations in soil-structure interaction problems (Atkinson, 2000). Despite its drawback in estimating ground/structure movements, the failure criterion of the MC model is still considered reliable for practical engineering purposes in predicting the stability of geotechnical problems, provided that correct strength parameters are adopted.

It is noted that more complicated soil stress-strain behaviors can be included in the MC model. Potts & Zdravkovic (1999) implemented a non-linear elastic and non-associated plastic MC model. Below the MC yield surface, the non-linear variation of soil stiffness with stress and strain levels (i.e., small strain stiffness) can be incorporated (e.g., Duncan & Chang, 1970; Jardine et al., 1986; Jurecic et al., 2013).

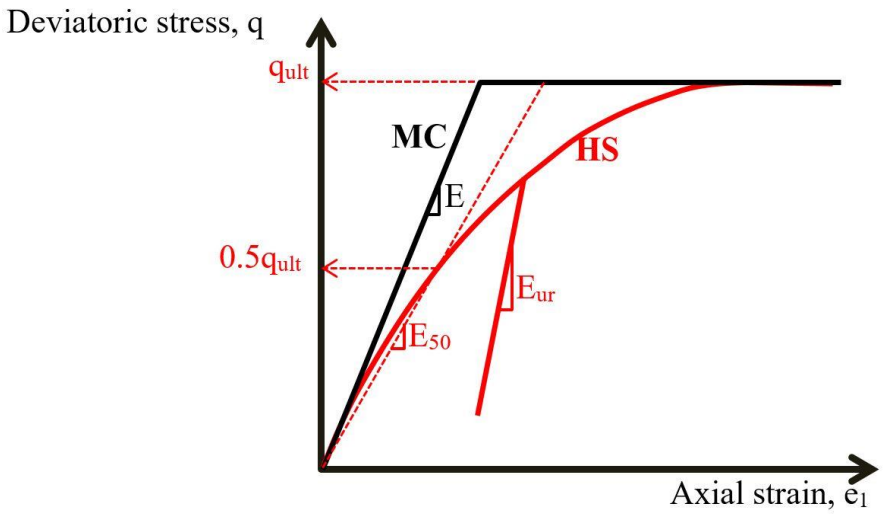


Figure 1. Stress-strain-strength behavior of the MC and HS models in drained triaxial test.

The Hardening Soil Model

The HS model is an isotropic hardening constitutive model that considers three different stiffness parameters as summarized in Table 1. Failure/the limiting condition for shearing is still governed by the Mohr-Coulomb failure criterion. The HS model is based on the classical plasticity theory, where for every stress increment there is a corresponding increase in elastic and plastic strains when undergoing primary loading and only elastic strain when unloading or reloading. Unlike nonlinear elastic models such as Duncan & Chang (1970), the HS model incorporates the theory of plasticity and includes soil dilatancy and a yield cap (PLAXIS, 2019). The yield surface can expand due to shear hardening and/or volumetric hardening. Comparing to the MC model, the HS model has the following additional features that better model the behavior of soils (PLAXIS, 2019):

(i) Non-linear stress-strain behavior prior to failure, which is similar to the hyperbolic curve by Duncan & Chang (1970);

(ii) Mean stresses generated plastic volumetric strains (Figure 2) with an associated flow rule assumed for volumetric yield locus;

(iii) Shear stresses generated plastic shear strains and plastic volumetric strains (Figure 2) with a non-associated flow rule assumed for shear or deviatoric yield locus;

(iv) Mobilizing dilatancy before failure; and

(v) Stress-dependent soil stiffness.

Schanz et al. (1999) describe the formulation and verification of the HS model. The HS model adopts stress-dependent stiffnesses given by the following equations:

$$E_{50} = E_{50}^{ref}\left(\frac{c'\cos\phi' + \sigma'_3\sin\phi'}{c'\cos\phi' + p_{ref}\sin\phi'}\right)^m \tag{4}$$

$$E_{oed} = E_{oed}^{ref}\left(\frac{c'\cos\phi' + \sigma'_1\sin\phi'}{c'\cos\phi' + p_{ref}\sin\phi'}\right)^m \tag{5}$$

$$E_{ur} = E_{ur}^{ref}\left(\frac{c'\cos\phi' + \sigma'_3\sin\phi'}{c'\cos\phi' + p_{ref}\sin\phi'}\right)^m \tag{6}$$

Table 1. Input parameters for the MC and HS models.

Parameters	MC Model	HS Model
Effective friction angle, ϕ' (°)	✓	✓
Effective cohesion, c' (kPa)	✓	✓
Dilation angle, ψ (°)	✓	✓
Young's modulus, E (kPa)	✓	
Poisson's ratio, ν (-)	✓	✓
E_{50}^{ref} (kPa)		✓
E_{oed}^{ref} (kPa)		✓
E_{ur}^{ref} (kPa)		✓
Power for stress-dependent stiffness, m (-)		✓
Failure ratio, R_f (-)		✓
Reference pressure, p_{ref} (kPa)		✓

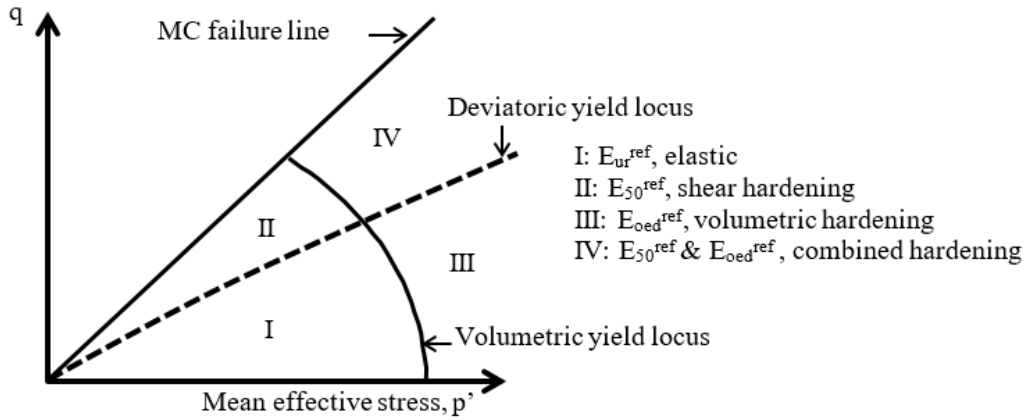


Figure 2. Double yield loci of the HS model.

Determination of Input Parameters of the Hardening Soil Model

Schanz et al. (1999) and Lees (2012) describe the sources of determining the input parameters of the HS model through laboratory tests. These sources are presented in Table 2.

Table 2. Determination of the key HS model input parameters from laboratory test.

HS Model Input Parameters	Sources from Laboratory Tests
E_{50}^{ref}	Secant stiffness in isotropically consolidated drained triaxial compression test at reference confining stress p_{ref}
E_{oed}^{ref}	Tangent stiffness for primary oedometer loading at reference vertical stress p_{ref}
E_{ur}^{ref}	Drained triaxial compression test with unload/reload loop at reference confining stress p_{ref}
m	The above tests undertaken at different confining stresses

Typical ranges of and relationships between the input parameters of the HS model have been developed based on experimental data. Some examples are given below.

(i) $E_{oed}^{ref} \approx E_{50}^{ref}$ for sands (Schanz & Vermeer, 1997) and $E_{oed}^{ref} \approx 0.5E_{50}^{ref}$ for soft clays can be assumed when oedometer test data is unavailable.

(ii) For sands, the $E_{ur}^{ref}/ E_{50}^{ref}$ ratio usually ranges from 3 to 6 for loose sand, and 2 to 4 for dense sand (Obrzud & Truty, 2018). For clays, the $E_{ur}^{ref}/ E_{50}^{ref}$ ratio usually ranges from 3 to 6. An $E_{ur}^{ref}/ E_{50}^{ref}$ ratio of 3 is usually adopted as a first-order approximation when triaxial test data is unavailable.

(iii) Power for stress-dependent stiffness (m) is usually taken as 0.5 for sands and gravels, 0.75 for silts, and 1.0 for clays (Obrzud & Truty, 2018).

The determined soil stiffness from laboratory testing depends on the quality of the ground investigation, i.e., of retrieval, transportation, storage, sample disturbance, and testing. Moreover, properties measured in an element test in the laboratory may not be representative of the mass properties of the ground considering the heterogeneity of typical soils in Hong Kong (GEO, 2007). Thus, in addition to laboratory tests, the stiffness parameters are also obtained from field tests and back analyses of similar case histories for practical design applications.

A discussion on the back-analyzed HS model input parameters and the performance of the HS model in cases with cohesive soil was reported by Teo & Wong (2012), Phienwej et al. (2012), Likitlersuang et al. (2013), and Lim & Ou (2017). Similar discussion for cases in granular soil was reported in Hsiung & Dao (2014), Khoiri & Ou (2013), and

Huynh et al. (2019). Local studies from Hong Kong involving the use of the HS model were reported by Lu et al. (2018), Lee et al. (2008), and Lam (2018). Findings of their analyses are summarized below:

(i) Hsiung & Dao (2014) reported a case history of deep excavation in sands with back analysis using finite element methods with the MC and HS models. Hsiung & Dao reported an empirical correlation of E_{50}^{ref} = 1.2 × SPT-N (MPa) in the HS model (p_{ref} = 100 kPa), while in the MC model, E = 2 × SPT-N (MPa).

(ii) Khoiri & Ou (2013) reported that the E value of the MC model is approximately equal to the value of E_{ur} in the HS model, and $E_{ur}^{ref}/E_{50}^{ref} \approx 3$. In the HS model, a larger E_{ur}^{ref} value is necessary for the bottom soil layers to approximately represent the high soil stiffness at a very small strain level of 1×10^{-6}.

(iii) Local studies by Lu et al. (2018), Lee et al. (2008), and Lam (2018) reported that the correlations E_{oed}^{ref} = 0.7 to 1.0 E_{50}^{ref} and E_{ur}^{ref} = 2.0 to 3.0 E_{50}^{ref} are suitable for modeling the soils in Hong Kong.

Based on the above literature, the HS model was reported to be capable in providing better estimations of the wall deflection profile at lower depths, the ground surface settlement profile behind the wall, and the ground heave at the excavation base for the above cases.

More Advanced Constitutive Models Based on the Hardening Soil Model

For deep excavation problems involving unloading, the stress/overburden reduction inside cofferdam will result in the reduction of E_{ur} due to the reduction of σ'_1 and hence σ'_3. It has been reported that Equation [6] may give excessive reduction of E_{ur} due to its dependency on σ'_3, (Nejjar et al., 2019; PLAXIS, 2020). To address this problem, Nejjar et al. (2019) reported the use of the Generalized Hardening Soil (GHS) model, which is a modular version of the HS model that allows users to change the setting of strain and stress dependency. For example, E_{ur} in Equation [6] could be set to be dependent on pre-consolidation pressure (p'_c) and/or mean effective stress (p') in order to avoid the excessively large reduction of E_{ur} in unloading problems (Equations [7] and [8]).

$$E_{ur} = E_{ur}^{ref}\left(\frac{\{\sigma'_3 + p'_c\}/2}{p_{ref}}\right)^m \tag{7}$$

$$E_{ur} = E_{ur}^{ref}\left(\frac{\{p' + p'_c\}/2}{p_{ref}}\right)^m \tag{8}$$

The Hardening Soil Model with Small-Strain Stiffness (HSsmall) becomes an extension of the HS model by including the nonlinear soil stiffness from very small strains ($1x10^{-6}$), as shown in Figure 3. The HS model considers the degradation of soil stiffness from a strain level of approximately $1x10^{-3}$, i.e., the stiffness at very small strain level is not considered. In this paper, only the HS model will be used to analyze the two deep excavation case histories in Hong Kong, as the input parameters for the HS model are more commonly available in routine ground investigation and from laboratory testing. The performance of the GHS and HSsmall models may be investigated in further studies.

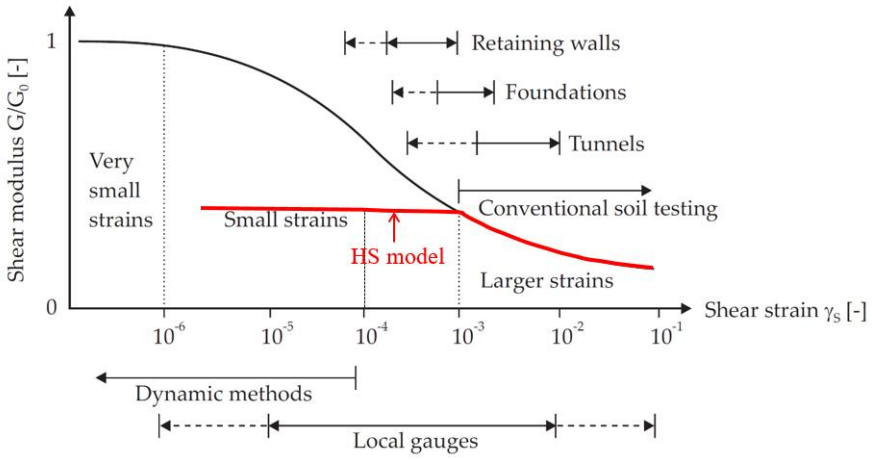


Figure 3. Modulus degradation curve of the HS model (after Benz, 2007).

METHODOLOGY

Under this study, back analyses were conducted using finite element models with the MC model and the HS model, based on the available monitoring data of the observed ground movements induced by deep excavations in Hong Kong. The findings of the study would be useful in assessing the applicability of the models in the design of deep excavations in Hong Kong.

Two deep excavation cases for the construction of Mass Transit Railway (MTR) stations were selected covering two types of excavation commonly seen in the urban settings of Hong Kong: (i) an excavation supported by embedded retaining walls with strutting, and (ii) an open excavation with temporary cut slopes. The first case is a 18 m deep excavation supported by strutted diaphragm walls for the construction of Tsuen Wan West (TWW) Station. The second one is an open excavation at Ho Man Tin (HMT) Station which is mainly comprised of the formation of a 48.5 m high temporary open cut slopes supported by soil nails. The locations of the two cases are shown in Figure 4.



Figure 4. Locations of the two cases studied shown on a map of Hong Kong (modified from map.gov.hk).

Two-dimensional plane-strain finite element models developed in PLAXIS 2D were adopted in the present study. The soil stiffness parameters for the soil constitutive models were calibrated by matching the predicted movements from the numerical models with the recorded ones.

For the MC model, the Young's Modulus E, which defines the slope of the linear stress-strain curve, was adopted as the only parameter for back analyses. For the HS model, the E_{50}^{ref} was chosen as a primary parameter for calibration in the back analyses, followed by estimating the values of E_{oed}^{ref} and E_{ur}^{ref}. A sensitivity analysis was undertaken to examine the effects of the ratios of E_{ur}^{ref} / E_{50}^{ref} and E_{oed}^{ref} / E_{50}^{ref} on the predicted ground movement for the two sites.

CASE 1 – STRUTTED EXCAVATION FOR CONSTRUCTION OF TSUEN WAN WEST STATION

The case history presented in this section is the TWW Station, constructed between the late 1990s and early 2000s. The site is located adjacent the shoreline of Tsuen Wan, Hong Kong, on both previously and recently reclaimed land. Pickles et al (2003) presented the project details of the excavation works of the site, which comprised approximately 600 m of cut-and-cover tunnels and a 400 m long station structure with an excavation depth of up to 20 m. Figure 5 shows the general view and the location of the site.



Figure 5. Excavation works taken place for Tsuen Wan West Station in 2001.

Ground and Groundwater Conditions

The layout plan of the site is shown in Figure 6. The site comprised three major portions, namely the Station, Northern Approach Tunnel (NAT), and Southern Approach Tunnel (SAT). Figure 6 also shows the demarcation of the new reclamation and old reclamation. The portion of seaward side (western) wall of the station structure near Grid Line 50 (GL50) is located at the boundary of the new reclamation and old reclamation.

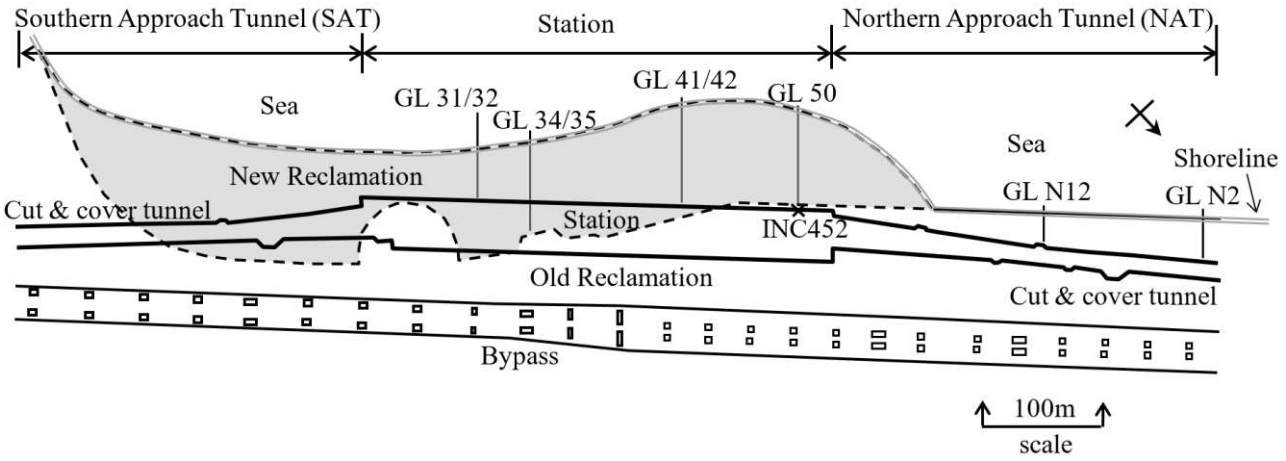


Figure 6. Layout plan of the Tsuen Wan West project (after Pickles et al, 2006); GL = grid line.

Pickles et al (2003) reported the ground conditions of the site. The stratigraphy consisted of fill overlying alluvium, completely decomposed granite (CDG), and granitic bedrock. The geological profile showing the seaward side of the tunnel and station structure before the new reclamation works is shown in Figure 7. The old reclamation had been completed more than ten years before the excavation works commenced. The fill in the older reclamation was composed of mostly general fill, a non-cohesive material with maximum particle size of less than 200 mm. A significant thickness of boulders or rockfill was also encountered, particularly in the area of former seawalls along the old shoreline, where soft clayey marine deposits were also dredged. The new reclamation works included the dredging of soft marine deposits, placement of fill and formation of the seawall. The fill in the new reclamation area was hydraulically placed, vibro-compacted marine sand. The alluvium underlying the fill or marine deposits was generally granular. Alluvial clay was encountered at some locations. Occasionally, cobbles and boulders were found inside the alluvium. The CDG generally consisted of silty sand with occasional gravel fragments.

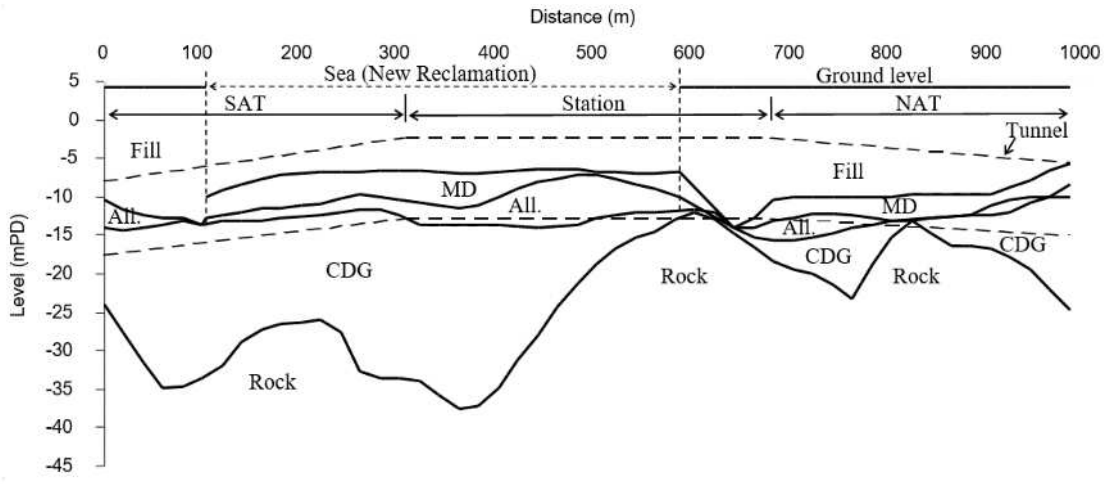


Figure 7. Geological profiles of Tsuen Wan West Station along the seaward side diaphragm wall before New Reclamation (after Pickles et al, 2006); All. = alluvium; MD = marine deposits; CDG = completely decomposed granite.

The Standard Penetration Test (SPT) values are often used to correlate with the stiffness of the ground for excavation designs in Hong Kong. The SPT-N values obtained from the ground investigation carried out on the old reclamation land are presented in Figure 8. The SPT-N value distribution of alluvium was more scattered, generally ranging from 4 to 80, indicating the variable nature of the soil. The SPT-N value distribution for CDG generally ranged from 10 to 90 across depth. A few exceptionally high SPT-N values of above 170 possibly indicated the presence of corestones derived from in-situ weathering of the parent rock. With respect to the old reclamation fill, it is noted that the distribution of SPT-N value for the old reclamation fill was generally uniform across depth ranges between 5 and 20. A few spikes in the N value of about 30 indicated possible hard inclusions within the fill layer. Nevertheless, it can be expected that the spatial variability of the fill material in the site was high, especially along the old seawall. Pickles et al (2003) reported that cobbles and boulders were found at the former seawall layer up to 8.0 m depth near the shoreline of the old reclamation. The SPT-N results for the marine sand fill placed in the newly reclaimed area are not available in the literature.

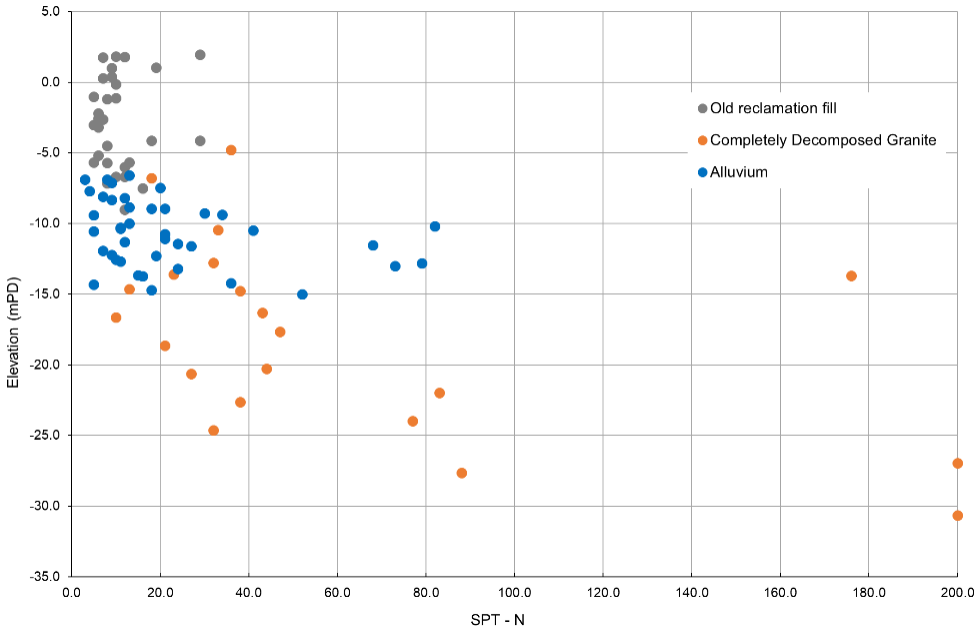


Figure 8. SPT-N value distribution of old reclamation fill, alluvium, and CDG.

The piezometric level fluctuated due to the tidal effect. Pickles et al (2003) reported that the magnitude of the piezometric response is a function of the distance of the piezometer from the seawall. The piezometric level recorded at seaward side of GL50 behind the wall during the construction period of the excavation and lateral support works (from Jan 2000 to

Oct 2001) fluctuated between +2.0 mPD and -1.2 mPD ("mPD" refers to meter above Principal Datum; 0.0 mPD is 1.3 m above mean sea level in Hong Kong).

Construction Method and Construction Sequence of the Cofferdam

The 42 m wide cofferdam for the station was supported by a pair of 1.2 m thick permanent diaphragm walls embedded in bedrock with two rows of temporary struts at a longitudinal spacing of 7.0 m. Subsequent to the completion of the new reclamation, pre-trenching was carried out at areas where the diaphragm wall construction was obstructed by the fill and alluvium containing a significant proportion of cobble and boulders. Details of the pre-trenching works are reported by Pickles et al (2003). Diaphragm wall construction was carried out after the pre-trenching works. Contact grouting was conducted to a depth of approximately 1 m below the toe of the wall embedded in rock. The contact grouting was used to improve the bearing capacity and reduce the local permeability of the rock.

A sectional view showing the construction sequence is presented in Figure 9. The construction of the station adopted a bottom-up approach. A two-stage pumping test was carried out to demonstrate the effectiveness of the water cut-off of the wall, as the site was located near the sea. The description of the construction stages, which is also denoted by the numbers in black circles in Figure 9, is shown in Table 3.

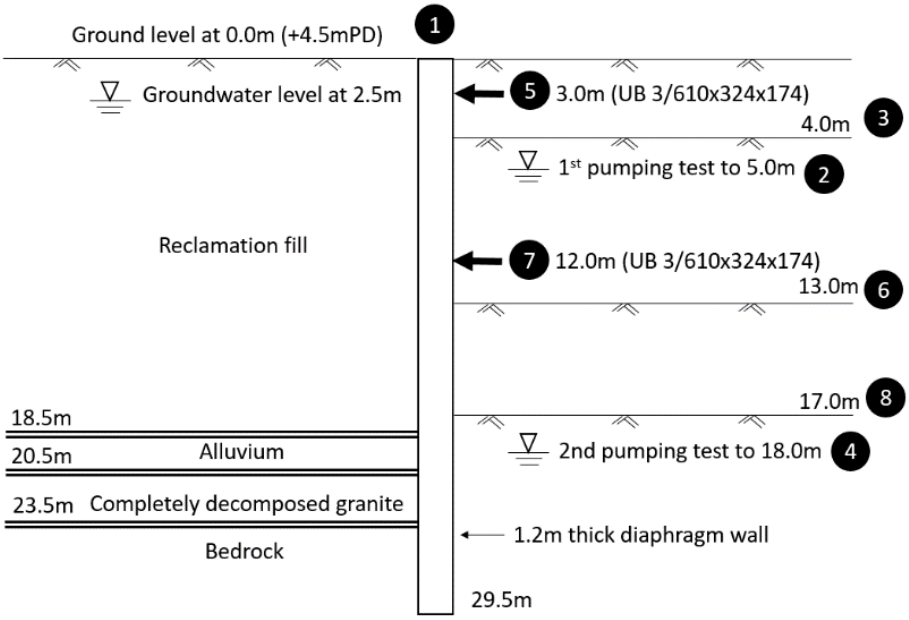


Figure 9. Construction sequence and geological profile at GL50, seaward side.

Table 3. Construction sequence of the excavation works at GL50, seaward side.

Construction Stage	Description
1	Pre-trenching, installation of diaphragm walls, and contact grouting
2	First stage pumping test to 5.0 m depth
3	Excavation to 4.0 m depth
4	Second stage pumping test to 13.0 m depth, groundwater level restored and maintained at 1.0 m below excavation level in subsequent stages
5	Installation of first row of struts at 3.0 m depth
6	Excavation to 13.0 m depth
7	Installation of second row of struts at 12.0 m depth
8	Excavation to 17.0 m depth to Final Excavation Level (FEL)

Monitoring Results

Instrumentations were installed to monitor the groundwater conditions and movement of the ground and diaphragm wall throughout the excavation works. The locations of these instruments at the GL50 seaward side—including a vibrating wire piezometer (VPZ449) with the response zone above rockhead in CDG located at 5 m behind the diaphragm wall, six ground settlement markers, and an inclinometer—are presented in Figure 10.

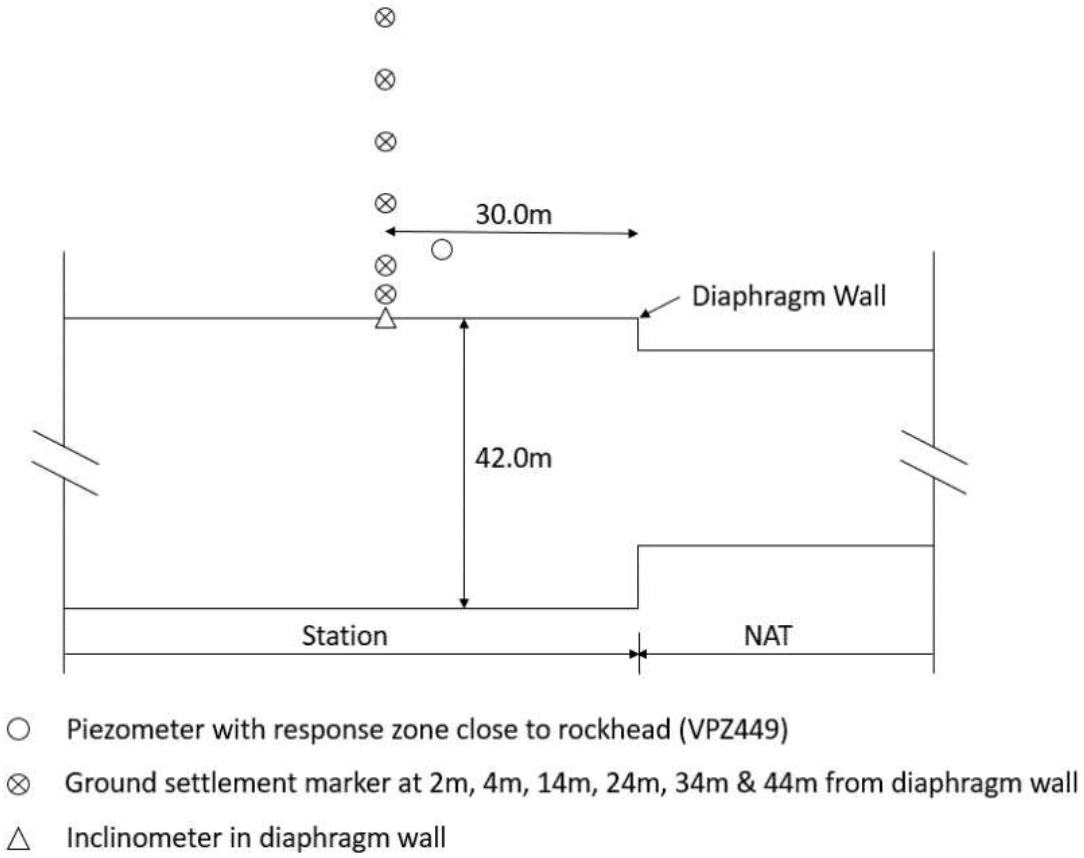


Figure 10. Instrumentations near GL 50, seaward side.

At the seaward side of GL50, groundwater monitoring through piezometer VPZ449 started one month before the installation of the diaphragm wall and continued throughout the excavation works. The maximum reduction of the piezometric head at VPZ449 during the entire course of excavation was around 0.5 m below the lowest recorded level. The small reduction was possibly owing to the proximity of the piezometer (and thus the seaward side of the excavation) to the sea with effective recharge of the groundwater regime. In addition, the embedment of the diaphragm wall in bedrock with contact grouting formed water cutoff, which further reduced the effect of groundwater drawdown due to dewatering and pumping test.

The measured lateral wall deflections and ground surface settlements up to the FEL are presented in Figures 11 and 12. The maximum lateral wall deflection occurred at 8.5 m depth (i.e., at half of the retained height) with a magnitude of 39 mm. The deflection reduced to a negligible magnitude at a depth of about -19.0 mPD (around 23.5 m in depth) owing to the stiff, competent bedrock in which the diaphragm wall is embedded. For the ground surface settlement, a concave type of settlement trough was observed with the maximum magnitude of 45 mm recorded at 4 m away from the wall. The trough extended to about 35 m behind the wall where the settlement recorded was less than 5 mm. It is noted that the distal end of the actual ground settlement profile between 35 m and 44 m remained flat with a magnitude of 4 to 5 mm without signs of tailing off. Given that the corresponding ground settlement recorded was small (about 4 mm), this could potentially be attributed to a combination of factors, such as the localized variation in the ground conditions and site activities proximate to the distal monitoring points.

The maximum lateral wall deflection and the maximum ground settlement correspond to about 0.23 % and 0.26 % of the retained height respectively. The maximum ground settlement to the maximum wall deflection ratio is about 1.1. The ratio of the extent of settlement trough to the depth of wall with zero deflection is about 1.4.

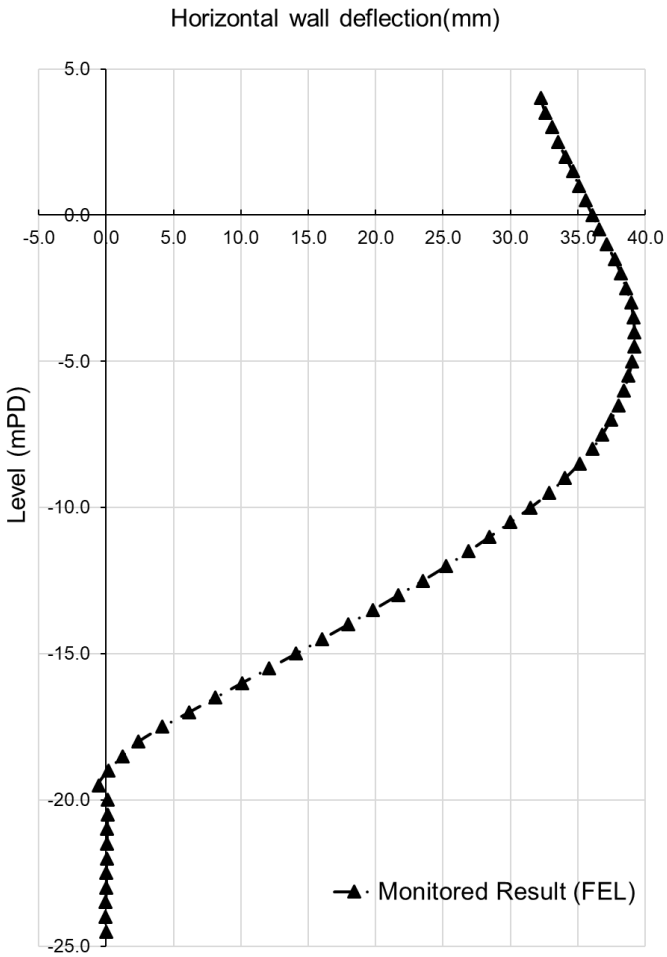


Figure 11. Wall deflection at GL50 seaward side at final excavation stage (after Pickles et al, 2003).

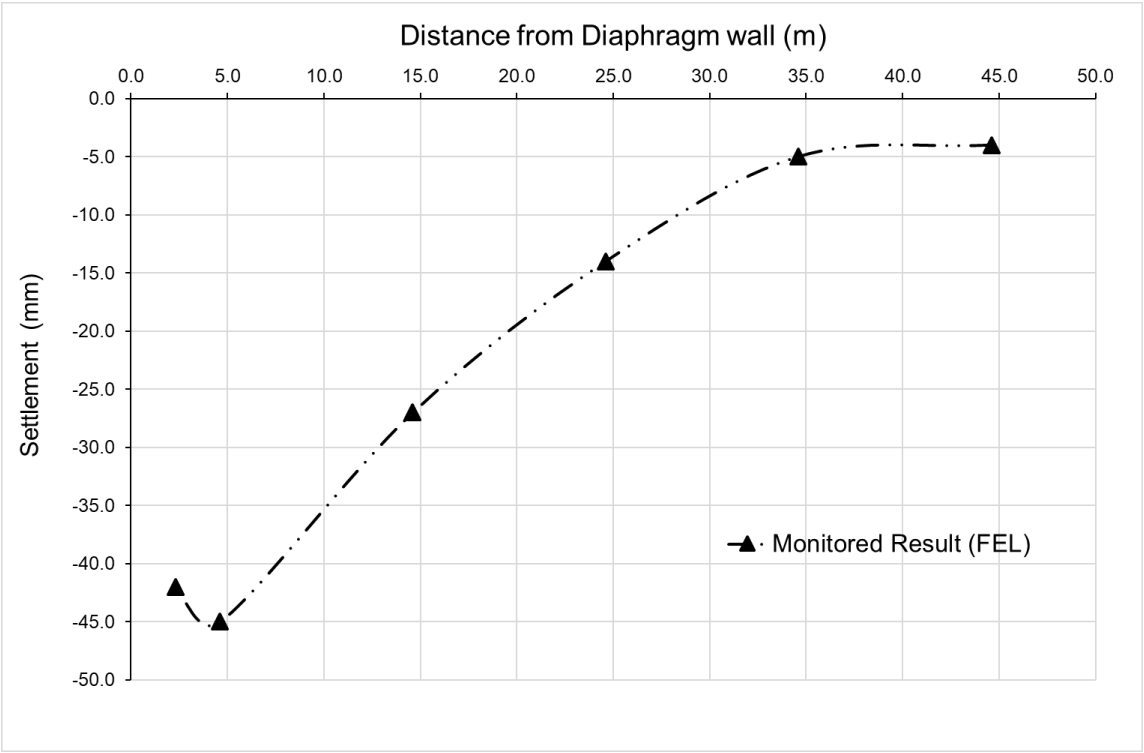


Figure 12. Ground settlement at GL50 seaward side at final excavation stage (after Pickles et al, 2003).

Finite Element Analysis Using Two Constitutive Models

A two-dimensional plane-strain finite element analysis was conducted to simulate the excavation at GL50 at the seaward side. The model geometry and finite element mesh are shown in Figure 13. 15-node finite elements were adopted. Plate elements with interfaces adopting a strength reduction factor for interface strength (R_{inter}) of 0.67 and fixed-end anchor elements were adopted to model the diaphragm wall and struts respectively. The input parameters of the structural elements are described in Tables 4 and 5. The highest measured piezometric head from VPZ449 was adopted in the model.

Table 4. Input parameters of diaphragm wall plate element.

	Unit	Diaphragm Wall
E_wA_w	kN/m	31.68×10^6
E_wI_w	kNm^2/m	3.802×10^6
D	m	1.2
Weight	kN/m^3	24.5
ν_w	/	0.15

Table 5. Input parameters of strut fixed-end anchor element.

	Unit	Strut
E_sA_s	kN	13.53×10^6
$L_{spacing}$	m	7.0

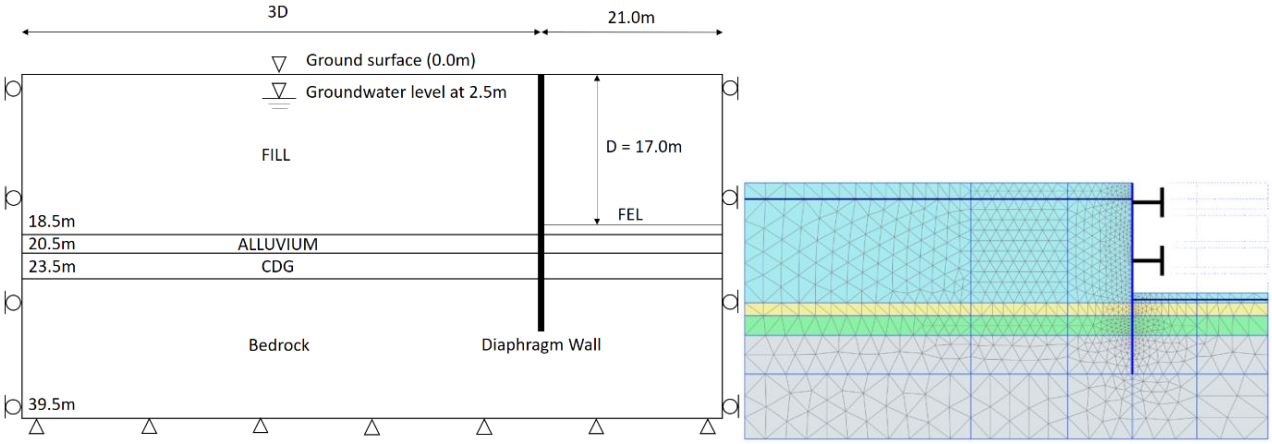


Figure 13. Finite element model for GL 50 at seaward side (FEL = Final Excavation Level).

The input parameters for the ground materials adopting the MC and HS models are presented in Table 6. For both the MC and HS models, the soil stiffness was back analyzed to match the predicted maximum lateral wall deflection with the monitored value. For all types of soil, the reference pressure for stiffnesses (p_{ref}) was set at 100 kPa and the power for stress-level dependency of stiffness (m) is 0.5, which is generally applicable to sands. The shear strength parameters were based on the isotropically consolidated undrained triaxial compression test results with pore water pressure measurement. There were no laboratory tests on shear strength for fill in the new reclamation area. The strength reduction factor for interface (R_{inter}) of 0.67 was adopted.

The bedrock was modeled as a linearly elastic material with E equal to 3 GPa with reference to the rock mass characteristics and the local design guidance. As there was no major piezometric drawdown on the retained side of the excavation throughout the works, the bedrock was also modeled as an impermeable material to simulate the actual monitoring results. For this reason, the wall deflection and ground settlement predicted by the MC model and the HS model can be solely due to the removal of soil and water within the cofferdam.

Table 6. Input parameters of the ground materials for the MC and HS models.

Soil	γ_{sat} (kN/m^3)	c' (kPa)	ϕ' (°)	HS Model					MC Model
				E_{50}^{ref} (MPa)	E_{oed}^{ref} (MPa)	E_{ur}^{ref} (MPa)	m	p^{ref} (kPa)	E (MPa)
Fill	19	0	34	$35x10^3$	$21x10^3$	$140x10^3$	0.5	100	$46x10^3$
Alluvium	19	0	34	$29x10^3$	$17x10^3$	$116x10^3$	0.5	100	$40x10^3$
CDG	19	0	37	$57x10^3$	$34x10^3$	$228x10^3$	0.5	100	$80x10^3$

Results of the Back Analysis

The predicted lateral wall deflection profiles are shown in Figure 14 and Table 7. Both the MC and HS models are able to match reasonably well with the maximum wall deflection and the deflection profile using the model parameters presented in Table 6. The depth where maximum lateral wall deflection occurs is around -4.8 mPD and -5.3 mPD for the HS model and the MC model respectively, whereas the actual depth of maximum lateral wall deflection is at -4.5 mPD. Both models slightly underpredicted the lateral deflection at the top of the wall, resulting in a slightly larger wall curvature at the final excavation stage.

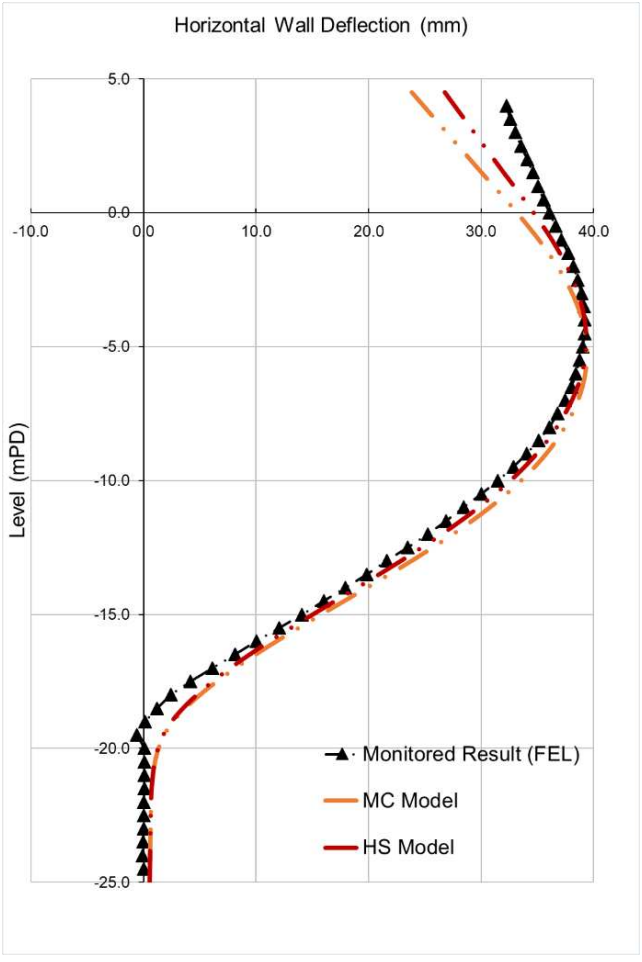


Figure 14. Horizontal wall deflection profiles of the MC and HS models plotted with inclinometer data at GL 50 seaward side.

After matching the wall deflection, the predicted ground surface settlement profiles from the MC and HS models are compared with the monitoring data. The results are shown in Figure 15 and Table 7. The MC model predicted the maximum settlement satisfactorily by deviating only by 0.3 mm, while the HS model gave a prediction of only 2.5 mm less than the observed value. The predicted maximum ground settlement occurred at 2.1 m and 4.1 m away from the centerline of the diaphragm wall for the MC model and the HS model respectively.

Compared with the actual ground settlement profile, the HS model performed better in predicting the location of the maximum ground settlement. Regarding the extent of the settlement trough, the MC model predicted a more confined trough which terminates distinctly at about 17 m away from the wall, which is equal to the excavation depth of 17 m. In contrast, the HS model produced a more extensive ground settlement profile, which exhibited a closer resemblance to the monitored field performance. In other words, despite that both the MC and HS models could reasonably predict the maximum ground settlement, the MC model significantly underpredicted the ground settlements at some distance behind the excavation.

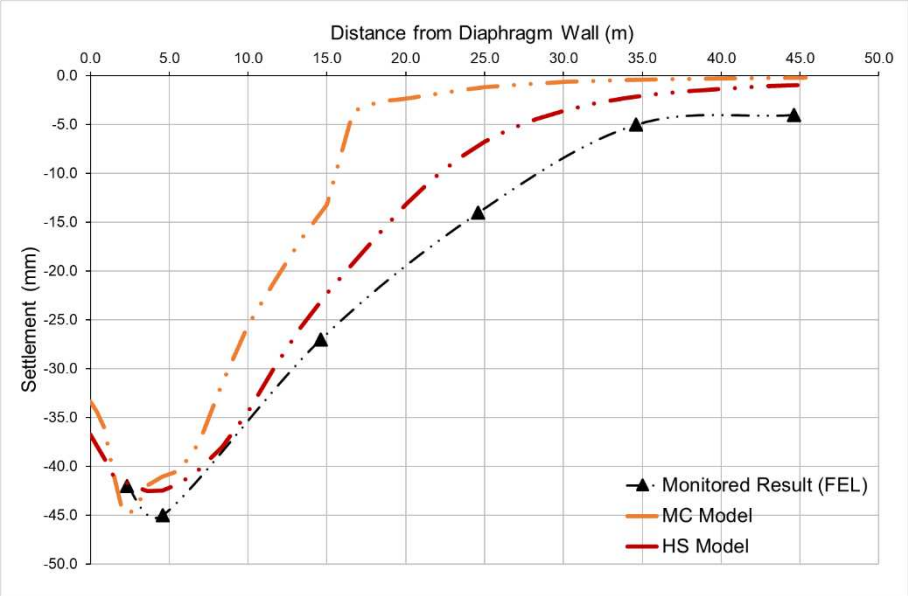


Figure 15. Ground settlement profiles of the MC and HS models plotted with ground settlement monitoring data at GL 50 seaward side.

Table. 7 Maximum wall deflection and ground settlement for the MC and HS models.

	Monitored Results	*MC Model*	*HS Model*
Maximum Wall Deflection	*39.2 mm*	*39.4 mm*	*39.3 mm*
Maximum Ground Settlement	*45.0 mm*	*44.7 mm*	*42.5 mm*

Sensitivity Study of HS Model Parameters

Regarding the HS model, a sensitivity study was carried out to examine the effect of the E_{oed}^{ref} and E_{ur}^{ref} on the modeled wall deflection and ground settlement. As the soil on the retained side comprised mainly fill material and the wall deflection mainly depended on the input parameters of the fill material, only the input parameters of the fill layer were altered for the sensitivity study. Five cases adopting different combinations of the ratio of $E_{ur}^{ref}/E_{50}^{ref}$ and $E_{oed}^{ref}/E_{50}^{ref}$, with the E_{50}^{ref} being kept constant at the calibrated value, were studied. These cases were established by changing one ratio while keeping another one unchanged. These combinations, as summarized in Table 8, are within the ranges reported in the literature for granular soils. It should be stressed that the results of this sensitivity study are only an observation from this particular case.

Table 8. Sensitivity study of stiffness moduli of fill using the HS model (p_{ref} = 100 kPa for all cases).

Case No.	$E_{oed}^{ref}/E_{50}^{ref}$	$E_{ur}^{ref}/E_{50}^{ref}$
Case A (Base Case)	0.6	4.0
Case B	0.6	2.0
Case C	0.6	6.0
Case D	1.0	4.0
Case E	1.4	4.0

The wall deflection profiles of Case A to Case E are presented in Figure 16. The maximum wall deflection shows a different sensitivity to the change in E_{oed}^{ref} and E_{ur}^{ref}. By reducing the E_{ur}^{ref} by half from 4.0 x E_{50}^{ref} to 2.0 x E_{50}^{ref}, the maximum lateral wall deflection increased by 9.7% from 39.3 mm to 43.1 mm. An increase in E_{ur}^{ref} from 4.0 x E_{50}^{ref} to 6.0 x E_{50}^{ref} resulted in a reduction of maximum wall deflection by 3% from 39.4 mm to 38.2 mm. With respect to the changes in $E_{oed}^{ref}/E_{50}^{ref}$, increasing the ratio from 0.6 to 1.0 and 1.4 reduced the maximum wall deflection to 39.0 mm and 37.6 mm respectively (0.8% and 4.3% of reduction). The shapes of the wall deflection profile remained generally the same for all five cases.

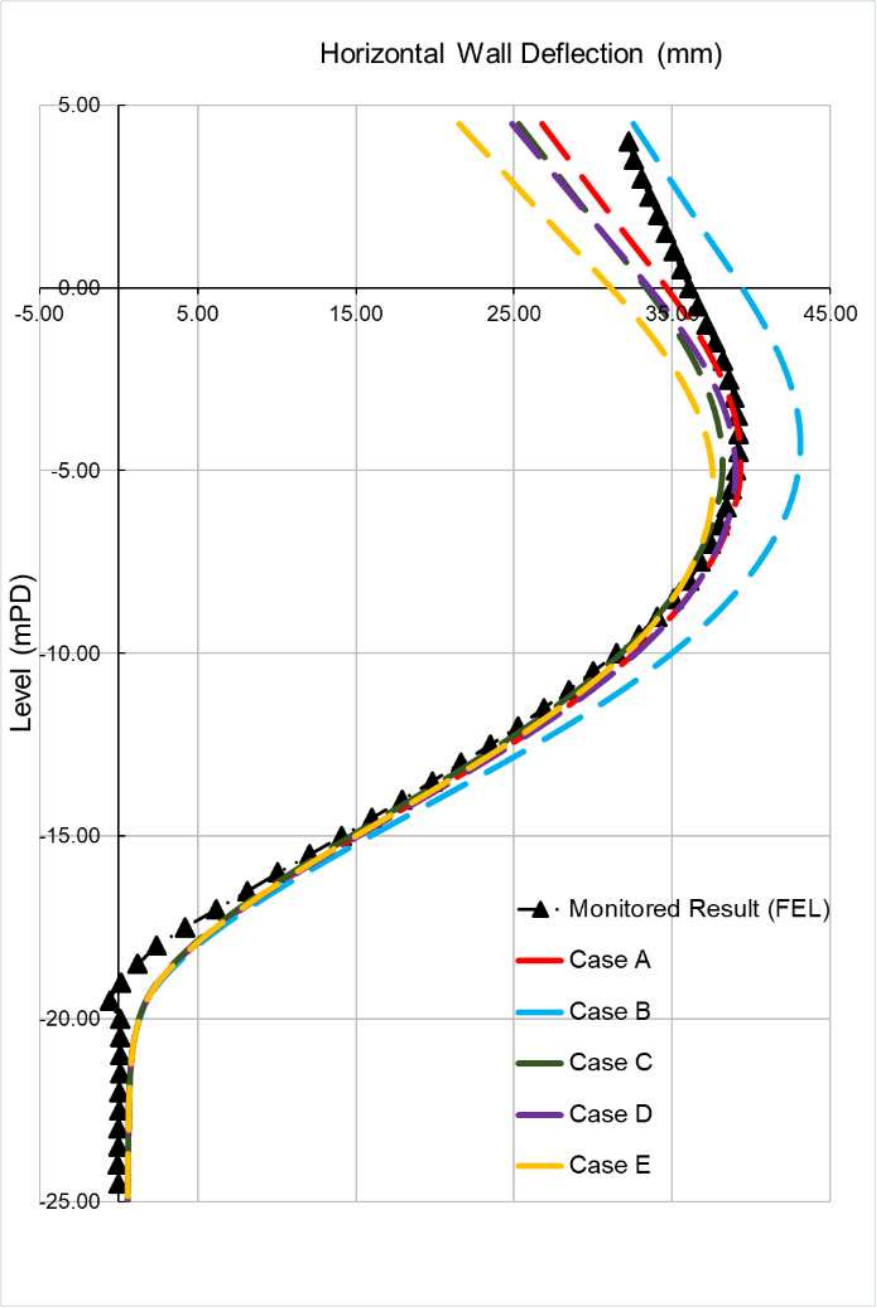


Figure 16. Horizontal wall deflection profiles of the HS models *for sensitivity study plotted with inclinometer data at GL 50 seaward side.*

The predicted ground settlement profiles of Case A to Case E are presented in Figure 17. A reduced E_{ur}^{ref} led to a slight increase in maximum ground settlement from 42.5 mm (Case A) to 43.1 mm (Case B), which amounted to a 1.4% increase. Yet the increase in E_{ur}^{ref} (i.e., Case C) did not affect the maximum ground settlement, as the ground settlement profiles for Case A and Case C were essentially identical. Increasing E_{oed}^{ref} to 1.0x E_{50}^{ref} (Case D) and 1.4 x E_{50}^{ref} (Case E) led to a significant reduction of maximum ground settlement by 7% and 14% respectively.

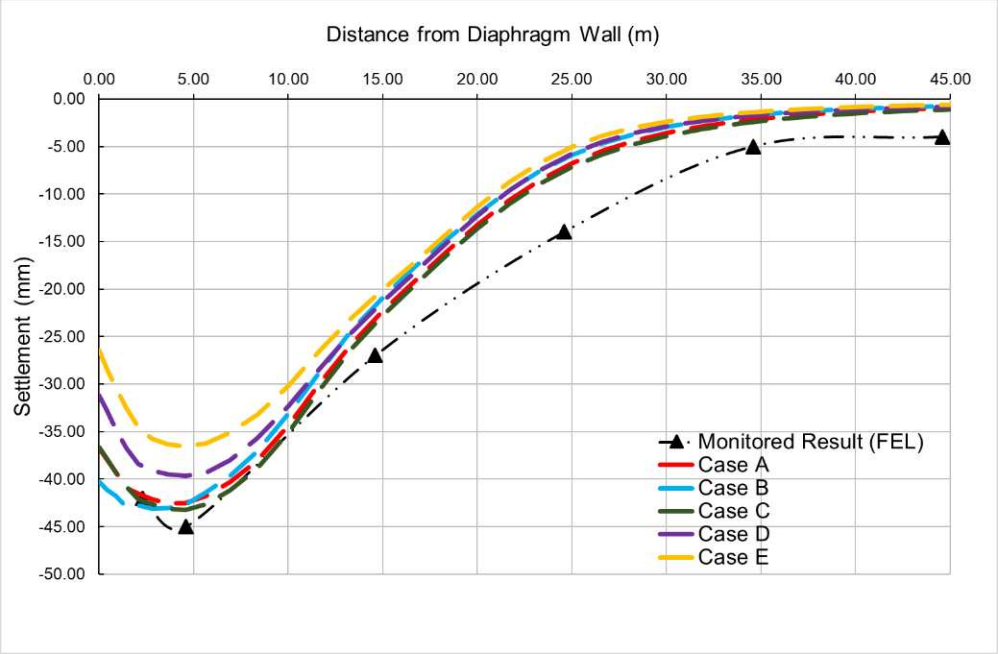


Figure 17. Ground settlement profiles of the HS model for sensitivity study plotted with ground settlement monitoring data at GL 50 seaward side.

CASE 2 – DEEP EXCAVATION FOR CONSTRUCTION OF HO MAN TIN STATION

The case history presented in this section is the site formation works for construction of the Ho Man Tin Station (HMT) in the Kwun Tong Line Extension Project. The site is located at the former Valley Road Estate, southeast of the No. 12 Hill which is a filled platform at +37 mPD. Kwong and Chim (2015) presented a performance review for the site formation works of the HMT which mainly comprised a phased open excavation with a maximum depth of about 50 m. Figure 18 shows the general view of the site formation works.

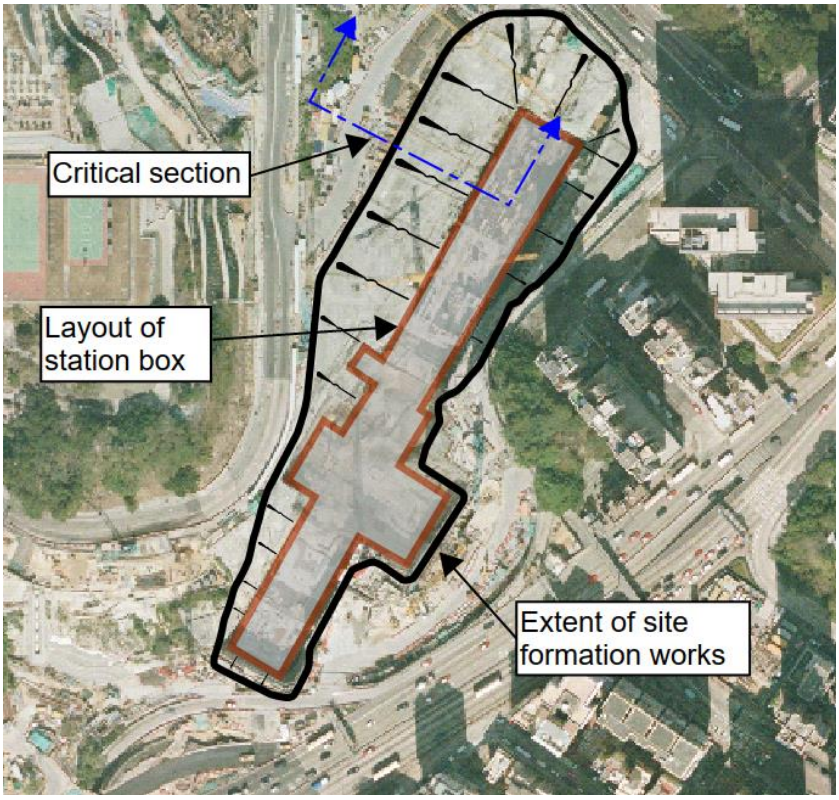


Figure 18. General view of the HMT excavation works.

Ground and Groundwater Conditions

Based on the interpretation of aerial photos taken since 1963, the site transverses across a northwest-southeast trending valley. The site was formed in the early 1960s by filling up the original valley to the level +37 mPD for the construction of the former Valley Road Estate development. The site was vacated since the demolition of the Estate in 2000 and reserved for the development of the HMT Station.

Figure 19 shows the general stratigraphy of the site before the excavation works. The site was underlain by fill consisting of loose to medium dense sand with varying degrees of silt, clay, and gravel. The thickness of fill varied with the topography of the original valley floor. A small amount of alluvium and colluvium was present at a localized area along the original valley floor. The maximum thickness of the fill was up to 27 m (with the bottom level at +10 mPD). The fill was underlain by medium-grained Kowloon Granite with various degrees of weathering. The Completely Decomposed Granite (CDG) material was about 10 m thick, comprised of sand with silt and gravel. The Highly Decomposed Granite (HDG) material was about 15 m thick, mainly comprised of gravelly sized rock fragments with quartz, sand, and silt materials. The SPT-N values of fill at the top 15 m varied from 5 to 20 and then became more scattered, ranging from 15 to 30 with a few exceptionally high values above 80, indicating the possibility of hard inclusions in the fill materials. The SPT-N values of CDG were also highly scattered, ranging from 30 to 90, indicating the heterogeneity of the material. The SPT-N results obtained from the ground investigation carried out are presented in Figure 20. Based on the available records, the existing groundwater level follows the existing hillside profile, and varies from +16 mPD to +20 mPD.

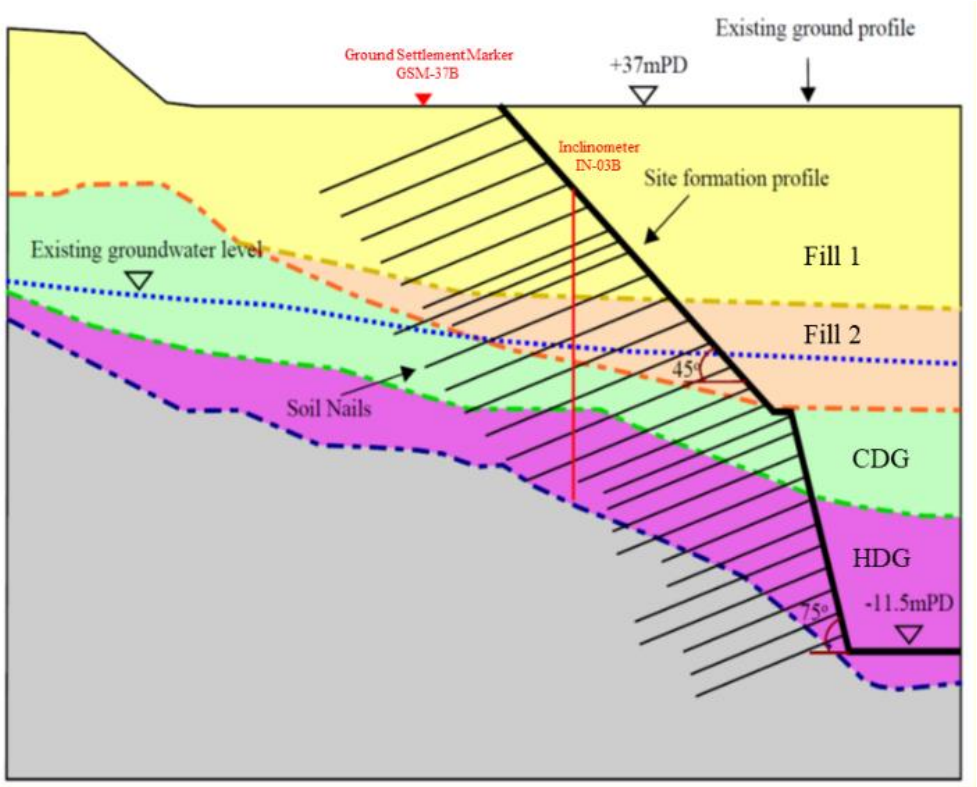


Figure 19. Cross-section of the HMT Station site.

Excavation Works

The construction sequence of excavation works is illustrated in Figure 21. It involves the formation of a 45° cut slope in fill and a 75° cut slope in saprolite. A total number of 26 rows of soil nails were installed. Shotcreting was being carried out on the slope surface throughout the excavation. The installation of soil nails was carried out following a specific construction sequence in stages. First, a 10 m high, 35° steep temporary cut slope was formed. Then, the temporary cut slope was further steepened to 45° with soil nails installed row-by-row until Row 5, meeting the toe level of the temporary cut slope. The excavation then proceeded down to the final formation level at -11.5 mPD with similar procedure, except that a 3 m wide and 2 m high berm was left unexcavated below each row of soil nail until its installation was completed. The same construction sequence was adopted for excavation below CDG, except the angle of the final slope profile was set to 75°.

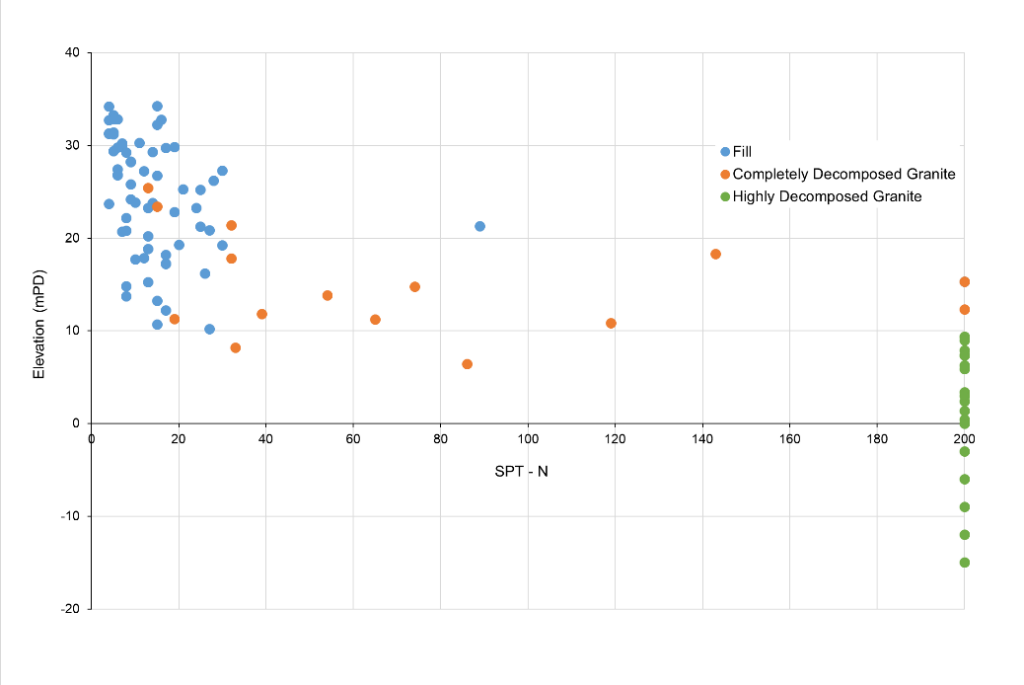


Figure 20. SPT-N value distribution of fill, CDG, and HDG.

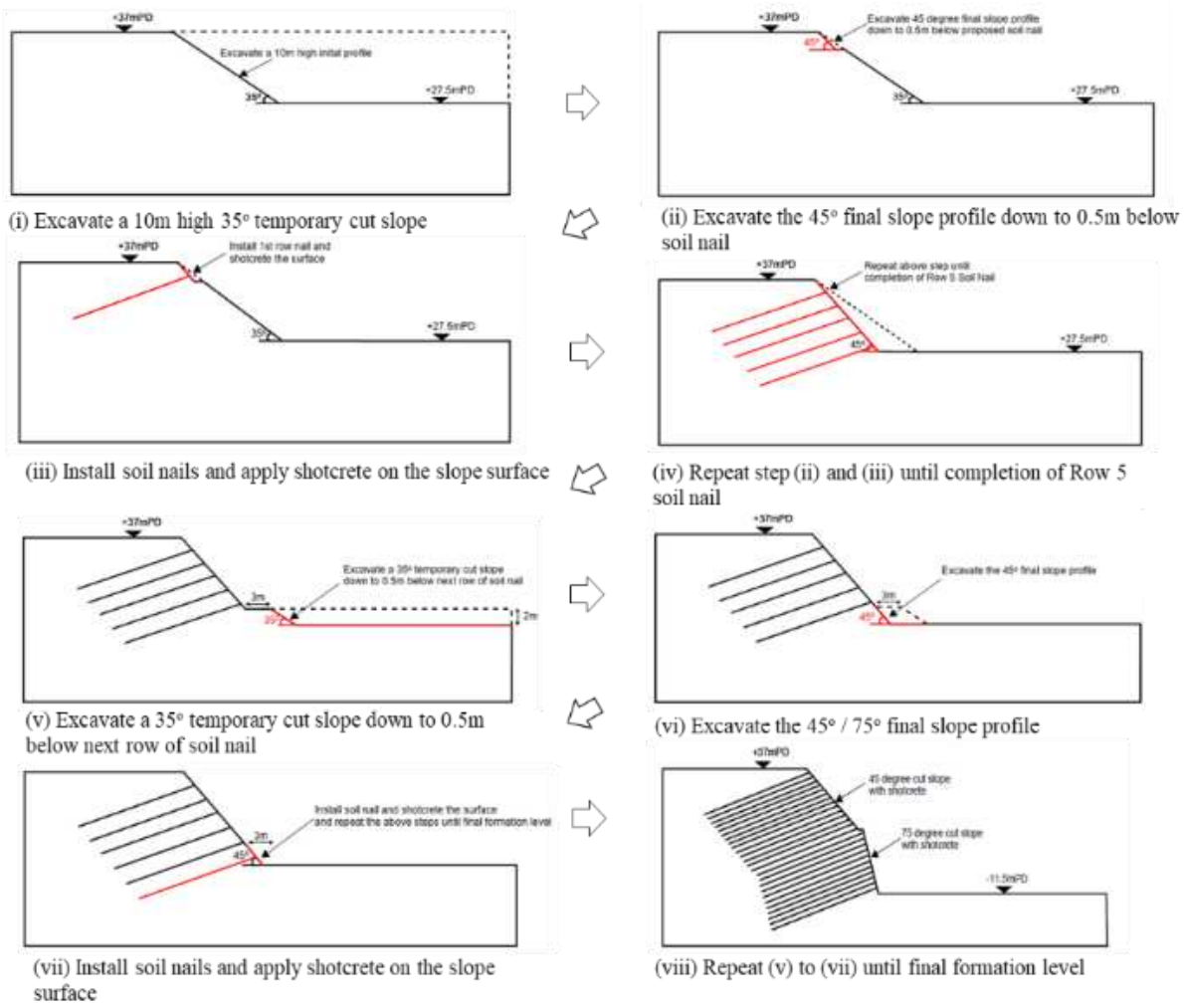


Figure 21. Construction Sequence of HMT site formation works.

Instrumentation Monitoring

Instrumentations were installed to monitor the movement of ground throughout the works. There were one ground settlement marker and two inclinometers installed near the section presented in Figure 19, in which their locations are also shown. Kwong and Chim (2015) reported the monitoring record of the ground settlement marker GSM-37B, which is located at about 5 m away from the slope crest. Kwong and Chim (2015) also referred to the monitoring records of inclinometer IN-03B, which was installed vertically at Row 4 of soil nail, for verifying the performance of the numerical models. The monitoring records of GSM-37B and IN-03B were used to review the performance of different numerical models in the coming sections.

Numerical Model

A two-dimensional plane strain finite element analysis was conducted at the critical section shown in Figure 19. 15-node finite elements were adopted. Kwong and Chim (2015) reported a significant lateral ground deformation was observed in the excavation of fill layer; therefore, a focused simulation of excavation in the fill layer has been carried out. The model geometry and finite element mesh of the numerical model are shown in Figure 22. The shotcrete and soil nails were modeled as a linearly elastic Plate element with a tensile stiffness of 22 GPa and a linearly elastic geogrid with a tensile stiffness of 40 GPa respectively. Interface elements between the shotcrete and soils with R_{inter} of 0.67 are included in the model.

The soil parameters adopted in the models are summarized in Table 9. For both the MC and HS models, the soil stiffness was back analyzed to match the predicted maximum lateral ground deflection with the monitored value at inclinometer IN-03B. For all types of soil, the reference pressure (p_{ref}) is set at 100 kPa and the power for stress-level dependency of stiffness (m) is 0.5, which is generally applicable to sands. The shear strength parameters were based on isotropically consolidated undrained triaxial compression test results with pore water pressure measurement in the same manner as the TWW case.

The bedrock was modeled as a linearly elastic material with E equaling 3 GPa with reference to the rock mass characteristics and the local design guidance.

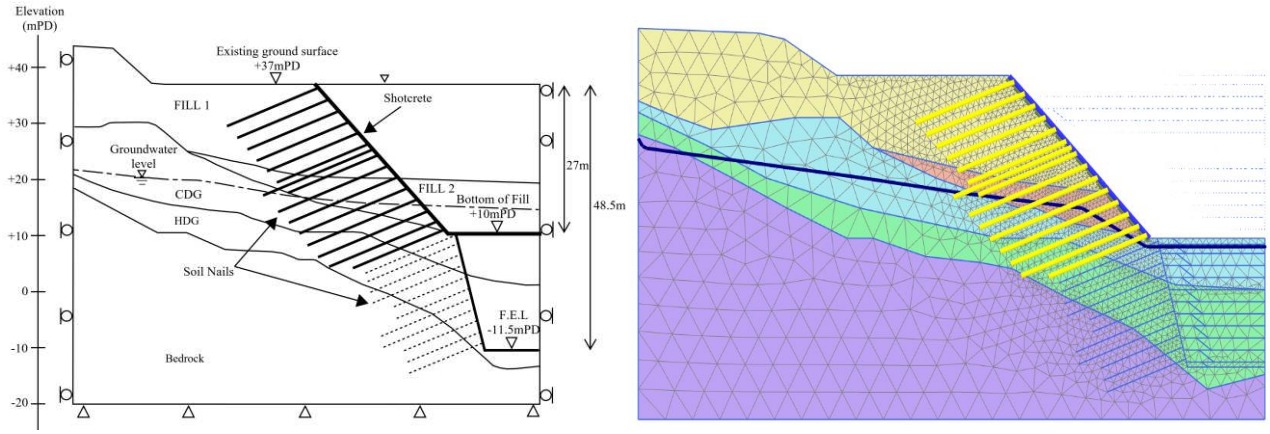


Figure 22. Finite element model for HMT Site formation.

Table 9. Summary of soil parameters.

Soil	γ_{sat} (kN/m^3)	c' (kPa)	ϕ' (°)	HS Model					MC Model
				E_{50}^{ref} (MPa)	E_{oed}^{ref} (MPa)	E_{ur}^{ref} (MPa)	m	p^{ref} (kPa)	E (MPa)
FILL 1	19	0	33	5x10^3	5 x10^3	15 x10^3	0.5	100	2 x10^3 + 150z [a]
FILL 2	19	0	35	20 x10^3	20 x10^3	60 x10^3	0.5	100	20 x10^3
CDG	19	5	39	50 x10^3	50 x10^3	150 x10^3	0.5	100	50 x10^3
HDG	19	100	40	200 x10^3	200 x10^3	600 x10^3	0.5	100	200 x10^3

[a] 'z' refers to the depth below ground in meters

Results of Analysis

Figure 23 shows the actual and predicted maximum lateral ground deflections at the location of inclinometer IN-03B until excavation down to bottom of the fill layer (i.e., +10.0 mPD). As the inclinometer IN-03B was located at the Row 4 soil nail at about +29.5 mPD, the monitoring records were only available after the excavation had proceeded to that level. Therefore, the incremental lateral ground deformations predicted by numerical models for excavation between +29.5 mPD and +10.0 mPD were compared with the actual site monitoring data. The results showed that both models gave a reasonably close estimate with the measured maximum lateral deformation.

The estimated ground settlements based on the MC model and the HS model at the location of ground settlement marker GSM-37B are shown in Figure 24, together with the actual monitoring data when reaching the bottom of the fill layer at +10 mPD. The MC model predicted a significant upward displacement of the ground. At the location of GSM-37B, the predicted ground heave was 30.8 mm. The HS model predicted a settlement of 64.5 mm at the same location. When compared with the actual monitored value of 63 mm, the MC model failed to predict the ground settlement, whereas the HS model gave a reasonably close estimate. Comparing the shape of the ground settlement profiles, the profile predicted by the MC model is irregular, with a maximum heave of 42.8 mm at about 2 m away from slope crest. The profile predicted from the HS model is of spandrel type, with the magnitude of settlement gradually reducing with the distance away from the excavation, and with a maximum predicted settlement of 121 mm at the slope crest.

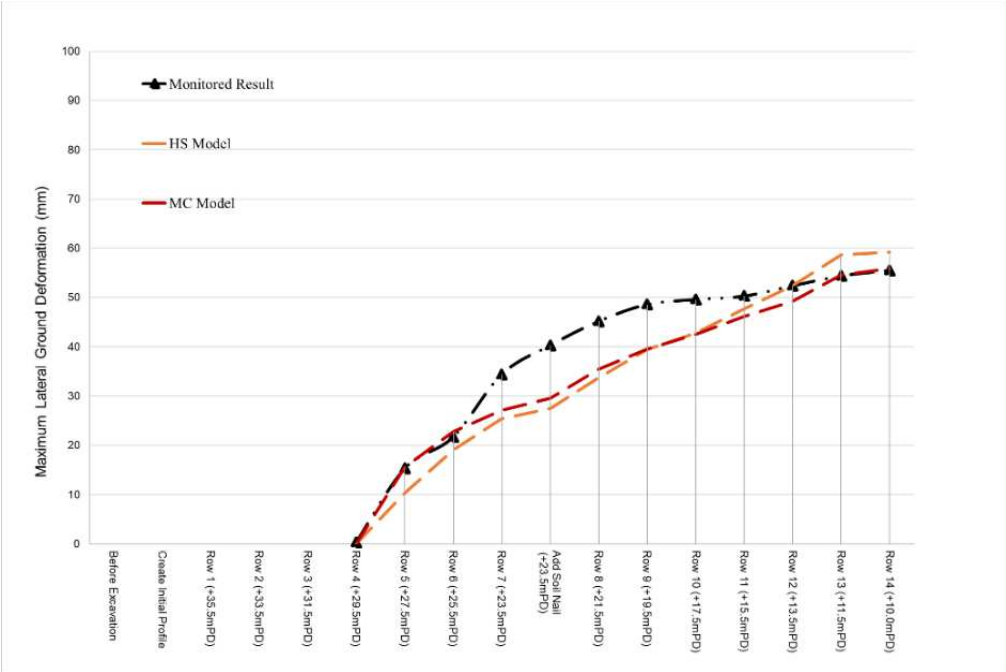


Figure 23. Maximum lateral ground deformation of the MC Model and the HS Model plotted with inclinometer IN-03B.

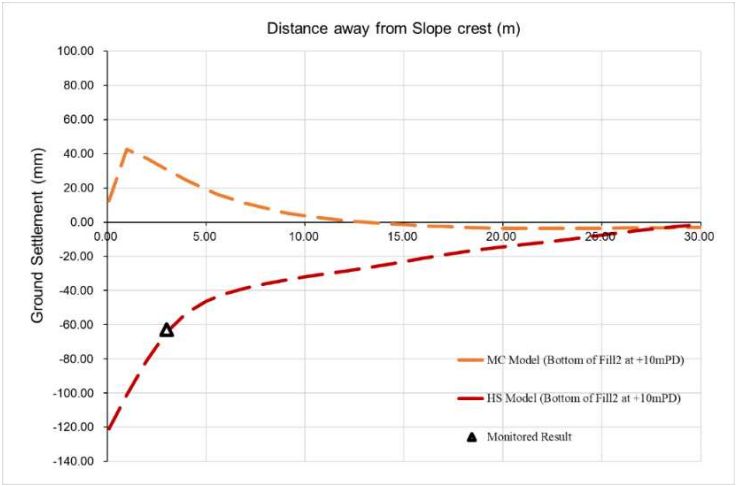


Figure 24. Ground surface settlement profile of the MC and HS Models plotted with the settlement data at slope crest.

Sensitivity Study of the HS Model Parameters

A sensitivity study to examine the sensitivity of the stiffness moduli, E_{ur}^{ref} and E_{oed}^{ref}, of the HS model was undertaken. The range of moduli adopted in the analysis was set by referring to the studies on modeling of soils in Hong Kong reported in the literature review (Table 10).

Table 10. Sensitivity study of stiffness moduli of fill using the HS model (p_{ref} = 100 kPa for all cases).

Case No.	$E_{oed}^{ref}/E_{50}^{ref}$	$E_{ur}^{ref}/E_{50}^{ref}$
A (Base Case)	1.0	3.0
B	0.7	3.0
C	1.0	2.0
D	1.0	4.0

The predicted maximum lateral ground deformation of Case A to Case D in comparison with the monitoring results are presented in Figure 25 and summarized in Table 11. The maximum lateral ground deformation shows different sensitivity to changes in E_{oed}^{ref} and E_{ur}^{ref}. By reducing the E_{ur}^{ref} from 3.0 x E_{50}^{ref} (Case A) to 2.0 x E_{50}^{ref} (Case C), the maximum lateral ground deformation increased significantly by 21.6% from 59.22 mm to 72.03 mm. An increase in E_{ur}^{ref} from 3.0 x E_{50}^{ref} to 4.0 x E_{50}^{ref} (Case D) resulted in a small increase in the maximum lateral ground deformation of 2.3% (from 59.22 mm to 60.56 mm). With respect to the changes in E_{oed}^{ref}, reducing the E_{oed}^{ref} from 1.0 x E_{50}^{ref} (Case A) to 0.7 x E_{50}^{ref} (Case B) resulted in a small reduction of maximum lateral ground deformation by 6.2% from 59.22 mm to 55.53 mm.

Table 11. Summary of sensitivity analysis results on maximum lateral ground deformation at Inclinometer IN-03B.

	Monitored Results (mm)	Case A (mm)	Case B (mm)	Case C (mm)	Case D (mm)
Maximum Lateral Ground Deformation	55.5	59.22	55.53	72.03	60.56

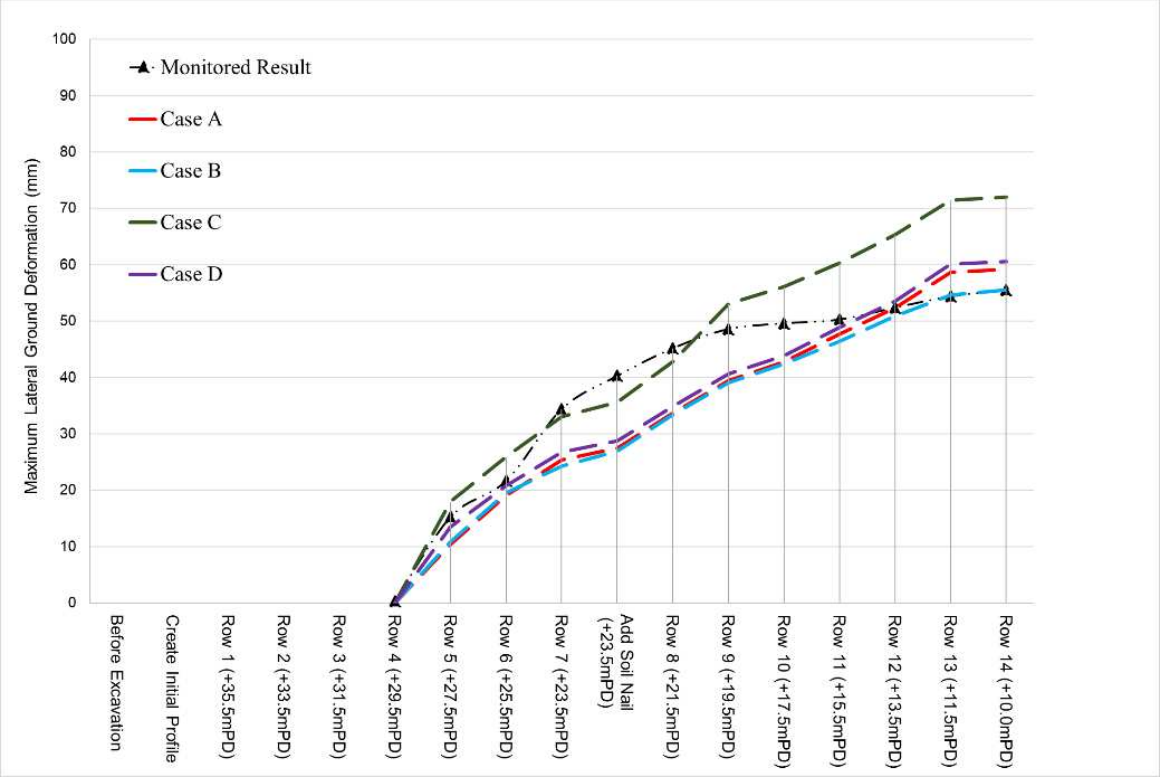


Figure 25. Sensitivity analysis on maximum lateral ground deformation in comparison with site monitoring records for HMT.

The predicted ground settlement profiles of Case A to Case D are presented in Figure 26 and Table 12. A reduction in E_{ur}^{ref} led to a small decrease in ground settlement by 4.6%, from 64.5 mm (Case A) to 61.56 mm (Case C), while increasing the E_{ur}^{ref} resulted in a substantial increase of ground settlement by 17.9% from 64.5 mm to 76.07 mm (Case D). Reducing E_{oed}^{ref} from 1.0 x E_{50}^{ref} (Case A) to 0.7 x E_{50}^{ref} (Case B) led to a notable reduction of ground settlement by 12.8% (from 64.5 mm to 56.27 mm).

Table 12. Summary of sensitivity analysis results on maximum lateral ground deformation at Ground Settlement Marker GSM-37B.

	Monitored Results (mm)	Case A (mm)	Case B (mm)	Case C (mm)	Case D (mm)
Maximum Ground Settlement	63.00	64.50	56.27	61.56	76.07

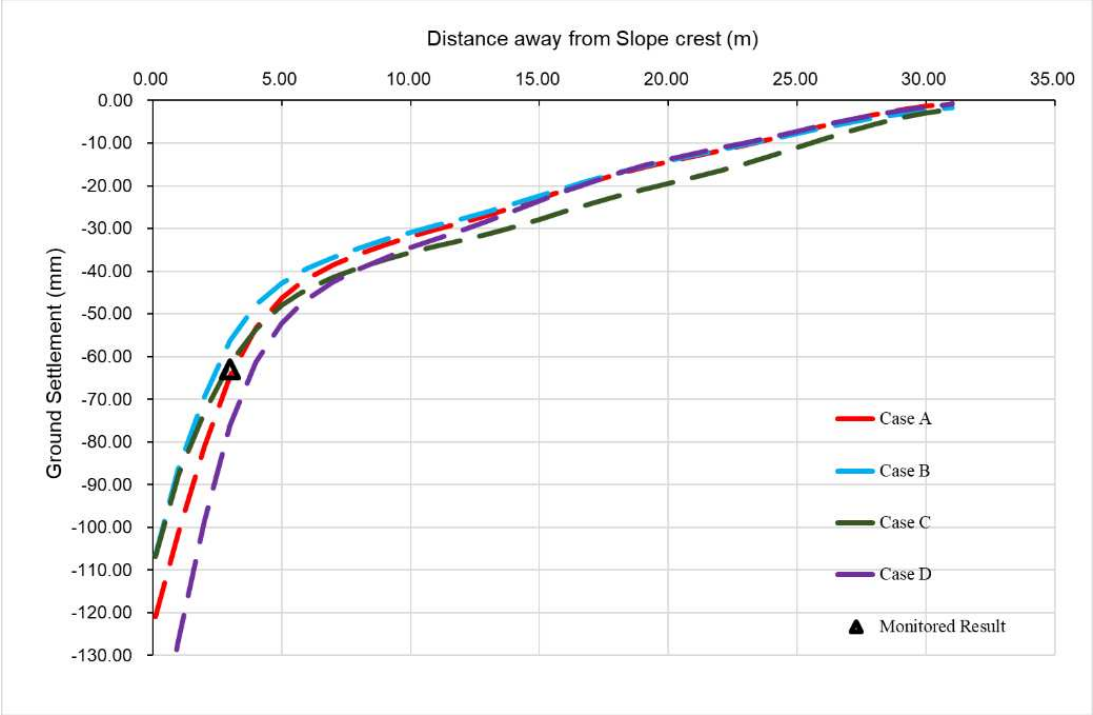


Figure 26. Sensitivity analysis on ground settlement in comparison with site monitoring records for HMT.

DISCUSSION

Predicted Lateral Wall Deflection

As observed in the section on the results on the numerical models of the TWW case, both the MC and HS models were able to predict the magnitude and location of the maximum lateral wall deflection generally well. However, both models underpredicted the lateral wall deflection above the first layer of strut (61% and 68% of the monitored deflection at the top of wall for the MC model and the HS model respectively), and slightly overestimated the wall curvature. This is consistent with the general observation in the literature (Lees, 2016) and the local experience (Chan, 2003) that the MC model with suitable input parameters is adequate for predicting the structural forces of embedded retaining walls and the associated lateral supports for typical design against ultimate limit states. Similarly, for the HMT case, both models gave a reasonably close estimate on the maximum lateral ground deformation as compared to the measured values.

Predicted Ground Surface Settlement Profile

For the case of TWW supported by a strutted diaphragm wall, the magnitudes and locations of the maximum ground settlement predicted by the MC and HS models were both reasonably accurate for design purposes as compared to the measured values. However, the MC model significantly underpredicted the extent of the ground surface settlement trough and thus the magnitude of settlement at some distance behind the excavation. The degree of underprediction can be improved using the HS model instead.

For the HMT case, a significant ground heave at the slope crest was estimated by the MC model, while the HS model predicted a settlement at the same location which agreed well with the site monitoring records. Figure 28 illustrates the effective stress path in p'-q space, where $p' = (\sigma_1' + \sigma_2' + \sigma_3')/3$ and $q = \sigma_1' - \sigma_3'$, of the soil elements A and B, of which the location is shown in Figure 27.

For the excavation above the respective soil element, the soil element underwent unloading generally along the K_o compression line with both p' and q reducing due to the reduction in both the lateral and vertical stress (from Point A1 / B1 to Point A2 / B2 respectively). This unloading continued as the excavation proceeded until it reached a level below the respective soil element when there was a change in the direction of the stress paths. Therefore, the stiffness that describes the unloading-reloading behavior would significantly affect the ground movement estimation. As the MC model relies on a single set of elastic stiffness parameters (E and ν) to describe both the pre-yield virgin loading and unloading stress-strain behaviors, it generally overestimates the ground heave due to unloading. As a result, a smaller ground surface settlement would be predicted or even heave behind the slope crest in this case.

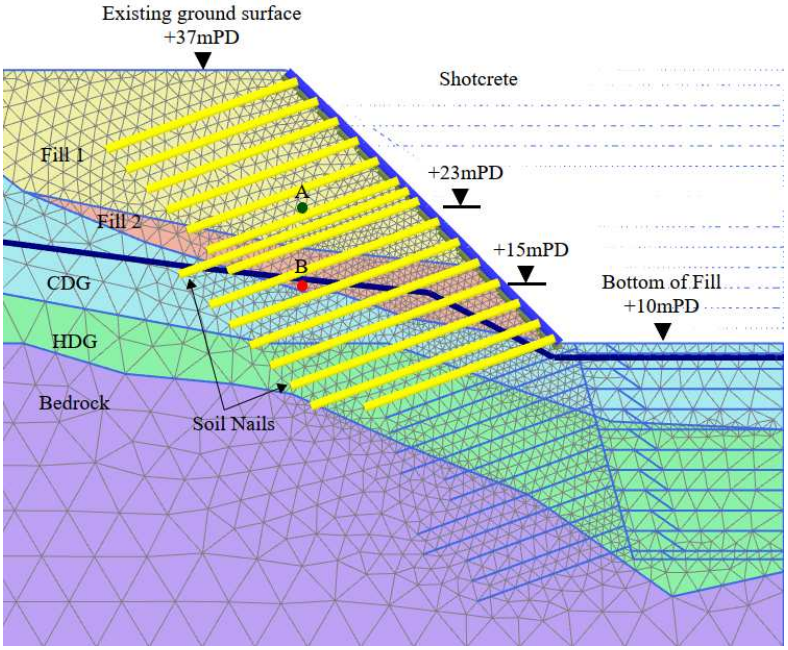


Figure 27. Position of soil elements A and B.

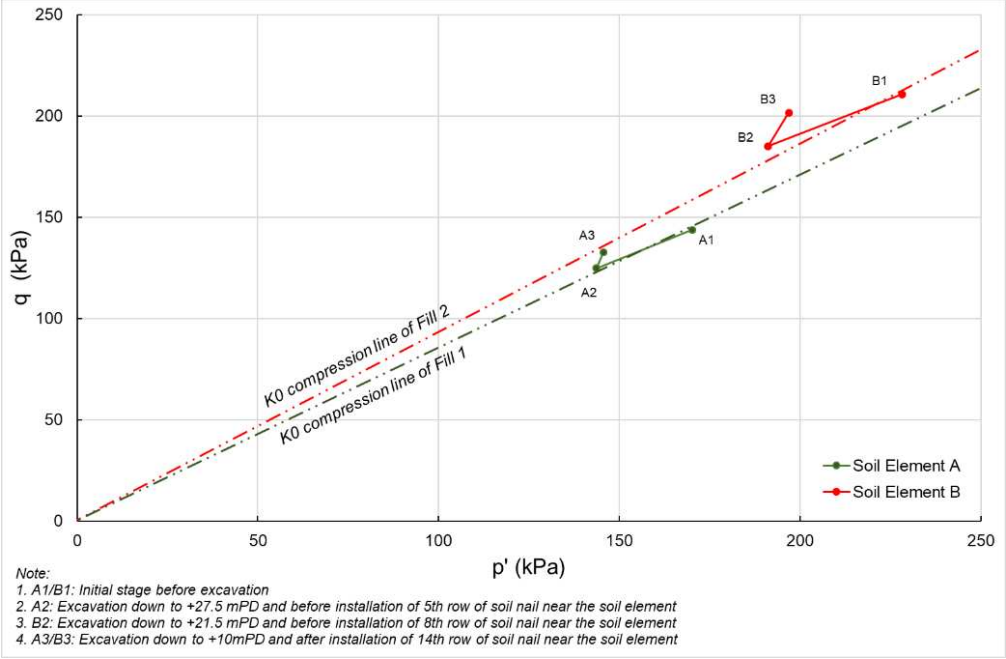


Figure 28. Stress paths from initial stage to final stage for soil element A (green) and B (red).

If we compare this with stress changes on the retained side of the excavation of the TWW case supported by an embedded retaining wall as illustrated by soil elements L and M (Figure 29), the elements experienced lateral stress reduction but effectively no change in the vertical stress due to excavation. This resulted in a different stress path (Figure 30) which goes into Zone II and/or Zone IV of the stress space shown in Figure 2. The elastic unloading is therefore not a dominating behavior on the retained side of the excavation (i.e., shearing is also involved), and thus the substantial predicted ground heave as predicted by the MC model in HMT case was not observed in the TWW case. However, another soil element N at the center of the excavation along the axis of symmetry underwent unloading in Zone I, which is mainly governed by E_{ur}^{ref}. As a result, the base heave predicted by the MC model in the TWW case is significantly higher than that predicted by the HS model (Figure 31).

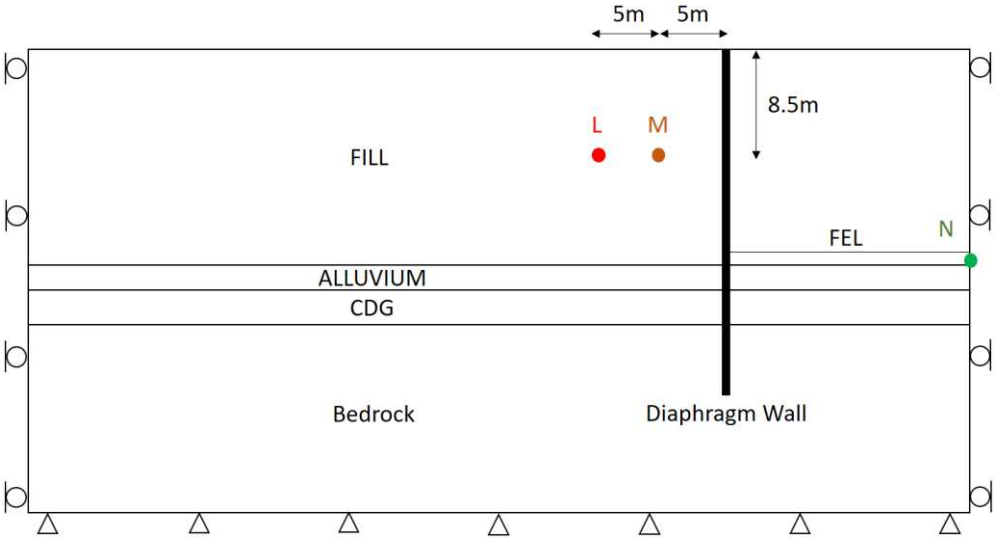


Figure 29. Position of soil element L (red), M (brown), and N (green).

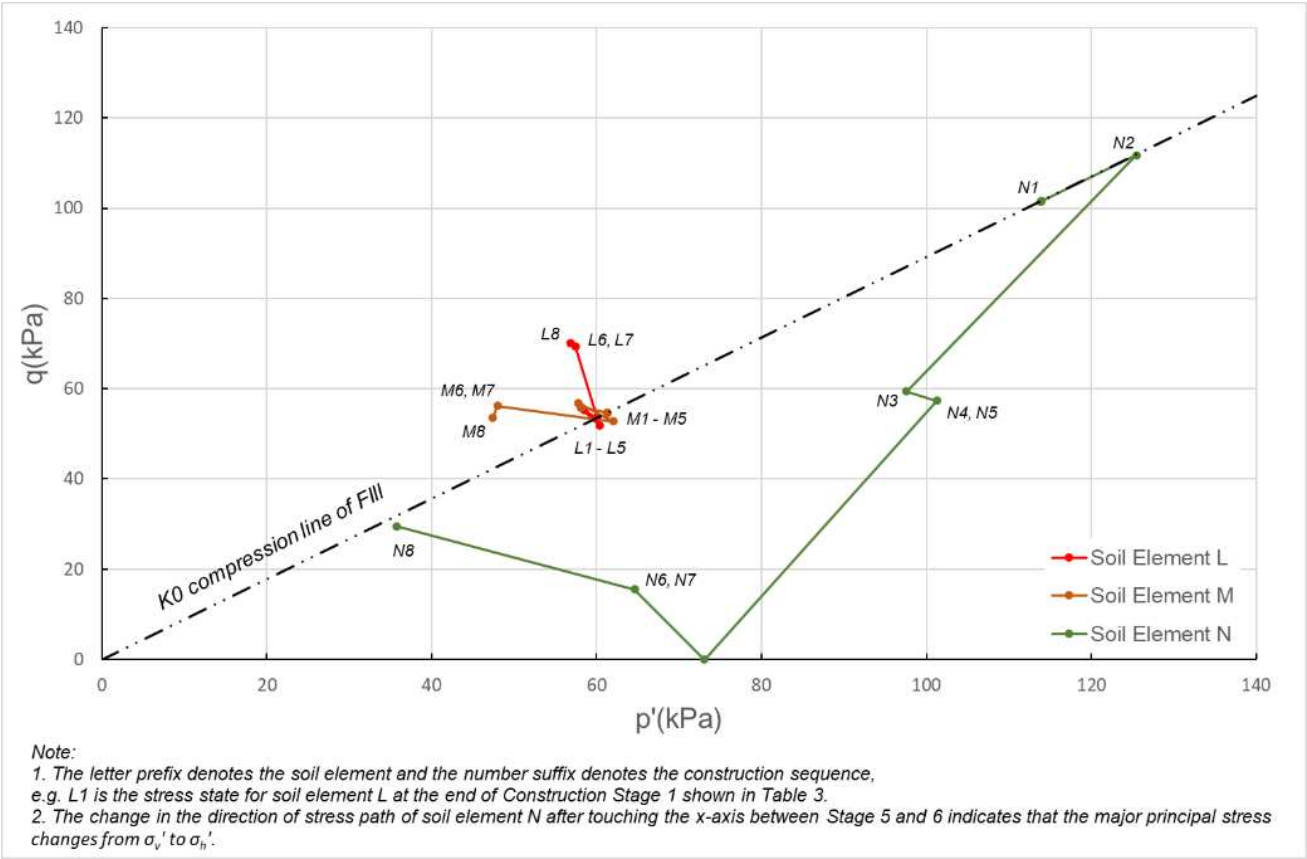


Figure 30. Stress paths from initial stage to final stage for soil element L (red), M (brown), and N (green).

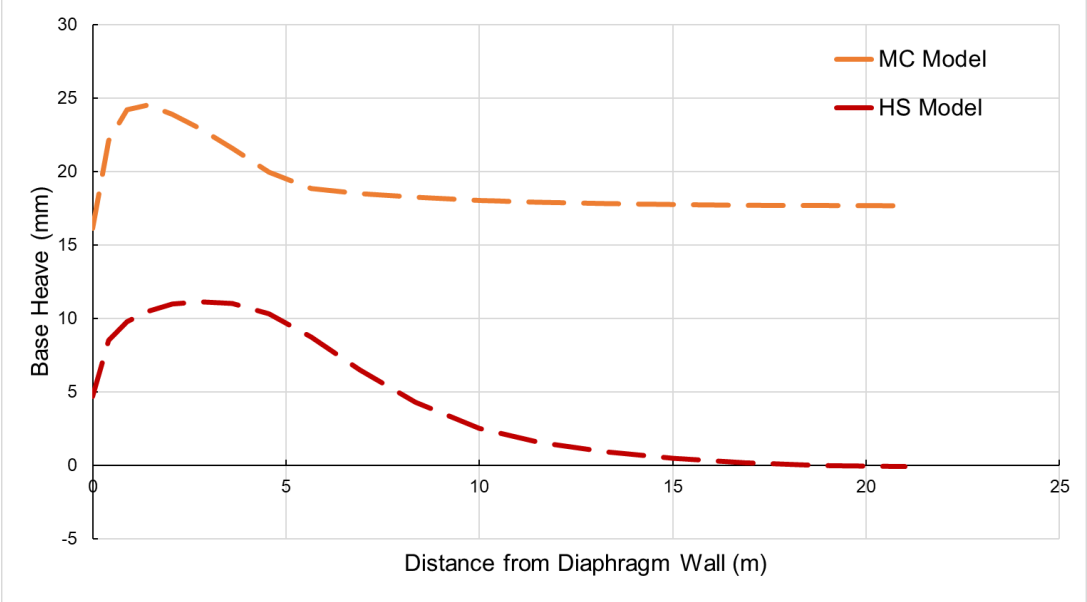


Figure 31. Base heave profile of the MC and HS models.

CONCLUSION

Two different deep excavation cases were selected for back analysis using the MC and HS models. Although with suitable stiffness parameters, the MC model provided a reasonable prediction on wall deflections and lateral ground movements for the geotechnical design of excavations, the potential of applying the HS model in practice, especially in improving ground surface settlement predictions, is demonstrated by this study. The improvement is mainly due to the ability of the HS model to consider nonlinear soil stiffness and unloading/reloading stiffness. Based on the back analysis, a set of relationships between the three stiffness parameters for the HS model were obtained for each case. It may serve as a useful reference for the selection of the parameters in similar settings.

For design purposes, the input E of the MC model and E_{50}^{ref}, E_{oed}^{ref}, and E_{ur}^{ref} of the HS model would need to be carefully selected with due consideration of factors such as the local soil properties, construction sequence, and workmanship, as well as the back analysis of well-documented local case histories of similar conditions.

ACKNOWLEDGMENTS

This paper is published with the permission of the Head of Geotechnical Engineering Office and the Director of Civil Engineering Development, the Government of the Hong Kong Special Administrative Region. The authors would like to acknowledge the MTR Corporation Limited for providing the inclinometer data of the HMT case.

REFERENCES

Atkinson, J. H. (2000). "Non-linear soil stiffness in routine design." *Geotechnique*, 50(5), 487-508.

Benz, T. (2007). *Small strain stiffness of soils and its numerical consequences*, PhD thesis, University of Stuttgart.

Bolton, M. D., Lam, S. Y., and Vardanega, P. J. (2010). "Predicting and controlling ground movements around deep excavations." *Keynote Lecture presented at Geotechnical Challenges in Urban Regeneration, the 11th International Conference of the DFI-EFFC*. London, 26–28 May, 2010, 30–47.

Chan, A. K. C. (2003). "Observations from excavations – a reflection." Case Histories in Geotechnical Engineering in Hong Kong, *Proc. of 23rd HKIE Geotechnical Division Annual Seminar*, 84-101.

Clayton, C. R. I. (2011). "Stiffness at small strain: research and practice." *Géotechnique,* 61(1), 5–37.

Dong, Y.P.. Burd, H.J., and Houlsby, G.T. (2016). "Finite-element analysis of a deep excavation case history." *Géotechnique,* 66(1), 1–15.

Duncan, J. M., and Chang, C. Y. (1970). "Nonlinear analysis of stress and strain in soils." *Journal of Soil Mechanics and Foundation Division*, Proceedings of the ASCE, SM5, 1629-1653.

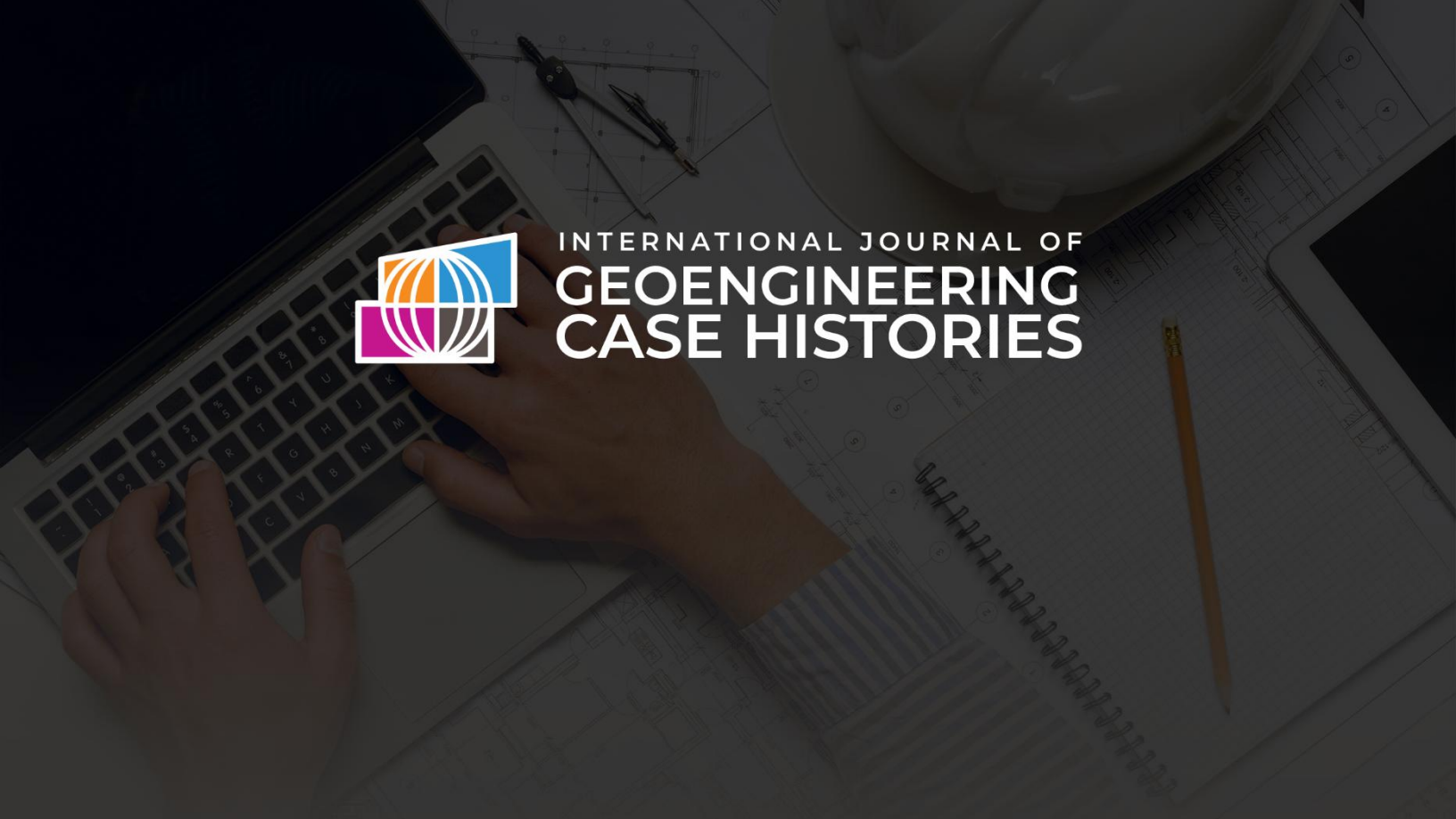
GEO (2007). "Engineering Geological Practice in Hong Kong (GEO Publication No. 1/2017)." Geotechnical Engineering Office, Hong Kong.

Hsiung, B. B. C., and Dao, S. D. (2014). "Evaluation of constitutive soil models for predicting movements caused by a deep excavation in sands." *Electronic Journal of Geotechnical Engineering*, Bundle Z4, 17325-17344.
Huynh, Q. T., Lai, V. Q., Tran, V. T., and Nguyen, M. T. (2019) "Back analysis on deep excavation in the thick sand layer by hardening soil small model." *Proc., International Conference on Sustainable Civil Engineering and Architecture 2019*, 659-668.
Jardine, R. J., Potts, D. M., Fourie, A. B., and Burland, J. B. (1986). "Studies of the influence of non-linear stress–strain characteristics in soil–structure interaction." *Geotechnique*, 36(3), 377-396.
Jurecic, N., Zdravkovic, L., and Jovicic, V. (2013). "Predicting ground movements in London Clay." *Proc. of the Institution of Civil Engineers, Geotechnical Engineering*, 166, GE5, 465-482.
Khoiri, M., and Ou, C. Y. (2013). "Evaluation of deformation parameter for deep excavation in sand through case histories." *Computer and Geotechnics*, 47, 57-67.
Kwong, A. K. L., and Chim, J. S. S. (2015). "Performance monitoring of a 50m high 75° cut slope reinforced with soil nail bars made from glass reinforced polymer (GFRP) at Ho Man Tin Station." *Proc., The HKIE Geotechnical Division Annual Seminar 2015*, 141-149.
Lam, A. K. M. (2018). "An engineering solution for a hillside project in Hong Kong." *ICE Publishing Geotechnical Research*, 5, 170-181.
Lee, S. W., Pickles, A. R., Henderson, T. O., and Li, E. S. F. (2008). "3D Modelling of deep excavation in decomposed granite influence of small strain stiffness and presence of individual piles." *Proc., The HKIE Geotechnical Division Annual Seminar 2008*, 171-180.
Lees, A. S. (2012). *Obtaining Parameters for Geotechnical Analysis*, NAFEMS, Glasgow, UK.
Lees, A. S. (2016). *Geotechnical Finite Element Analysis: a Practical Guide*, ICE Publishing, London, UK.
Likitlersuang, S., Surarak, C., Wanatowski, D., Oh, E., and Balasubramaniam, A. (2013). "Finite element analysis of a deep excavation: A case study from the Bangkok MRT." *The Japanese Geotechnical Society, Soils and Foundations 2013*, 53(5), 756-773.
Lim, A., and Ou, C. Y. (2017). "Stress paths in deep excavation under undrained conditions and its influence on deformation analysis." *Tunnelling and Underground Space Technology,* 63, 0217, 118-132.
Lu, K. K., Yin, J. H., and Lo, S. C. (2018). "Modelling small-strain behavior of Hong Kong CDG and its application to finite-element study of basement-raft footing." *International Journal of Geomechanics*, 2018, 18(9), ASCE.
Nejjar, K., Witasse, R., Dias, D., Cuira, F., and Burlon, S. (2019). "Accounting for nonlinear behaviour of ground for the prediction of settlements due to deep excavations." *Geotechnical Engineering Foundation of the Future, Proc. of XVII ECSMGE*, Reykjavik, 852-859.
Obrzud, R., and Truty, A (2018). *The hardening soil model – a practical guidebook*, Zsoil, the Switzerland.
Pickles, A. R., Lee, S. W., and Norcliffe, B. A. W. (2003). "Groundwater and ground movement around deep excavation." *Proc., Institution of Civil Engineers, Geotechnical Engineering* 156 July 2003, 147-158.
Pickles, A.R., Lee, S.W., and Sun, R.Y.F. (2006). "Ground movement of deep excavation in reclamation." *Proc., Danube European Conference on Geotechnical Engineering*, 2, 661–666.
PLAXIS (2019). *PLAXIS Material Models Manual 2019*, PLAXIS bv, The Netherlands.
PLAXIS (2020). "UDSM - Generalized Hardening Soil Model", <https://communities.bentley.com/products/geotech-analysis/w/plaxis-soilvision-wiki/46115/udsm---generalized-hardening-soil-model>.
Potts, D. M., and Zdravkovic, L. (1999). *Finite Element Analysis in Geotechnical Engineering: Theory*, Thomas Telford, London, UK.
Potts, D. M., and Zdravkovic, L. (2001). *Finite Element Analysis in Geotechnical Engineering: Application*, Thomas Telford, London, UK.
Phienwej, N., Humza, M., and Zaw Aye, Z. (2012). "Numerical modeling of diaphragm wall behavior in Bangkok soil using hardening soil model." *Geotechnical aspects of underground construction in soft ground*, 715-722.
Schanz, T., and Vermeer, P. A. (1997). "On the stiffness of sands." *Pre-failure deformation behavior of geomaterials*, 383-387.
Schanz, T., Vermeer, P. A., and Bonnier, P. G. (1999). "The hardening soil model: Formulation and verification." Beyond 2000 in Computational Geotechnics – 10 Years of PLAXIS International, Brinkgreve, R. B. J. (Ed.), 281-296.
Teo, P. L., and Wong, K. S. (2012). "Application of the hardening soil model in deep excavation analysis." *The IES Journal Part A: Civil & Structural Engineering*, 5, 152-165.

NOTATIONS

A_s	Sectional area of strut
A_w	Sectional area of wall
c'	Effective cohesion
c_u	Undrained shear strength
d	Thickness of wall

E	Young's modulus of soil
E_s	Young's modulus of strut
E_w	Young's modulus of wall
K_o	Coefficient of earth pressure at rest
$L_{spacing}$	Spacing of struts
p'	Mean effective stress
p'_c	Pre-consolidation pressure
p_{ref}	Reference pressure
q	Deviator stress
R_f	Failure ratio
R_{inter}	Strength reduction factor for interfaces
γ_{sat}	Saturated unit weight of soil
ν	Poisson's ratio
ν_w	Poisson's ratio of wall
σ'_1	Major effective principal stress
σ'_2	Intermediate effective principal stress
σ'_3	Minor effective principal stress
$(\sigma_1 - \sigma_3)_f$	Deviator stress at failure
σ'_v	Vertical effective stress
σ'_h	Horizontal effective stress
φ'	Effective friction angle
ψ'	Effective dilation angle



INTERNATIONAL JOURNAL OF
GEOENGINEERING
CASE HISTORIES

The Journal's Open Access Mission is generously supported by the following Organizations:

dar
a Sidara company

Geosyntec consultants
engineers | scientists | innovators

CONETEC
MUD BAY DRILLING
LANKELMA
Geotech DRILLING

ENGEO
Expect Excellence

Access the content of the ĪSSMGE Īnternational Journal of Geoengineering Case Histories at:
www.geocasehistoriesjournal.org

Downloaded: Wednesday, November 11 2026, 13:53:40 UTC